PATTERNS OF COMPUTED TOMOGRAPHY SCAN FINDINGS IN PATIENTS WITH SUPRAHYOID NECK MASSES AT THE MOI TEACHING AND REFERRAL HOSPITAL

NDUGIRE TITUS KARIUKI

A RESEARCH THESIS PRESENTED TO THE COLLEGE OF HEALTH SCIENCES, SCHOOL OF MEDICINE, MOI UNIVERSITY IN PARTIAL FULFILLMENT FOR THE AWARD OF MASTER MEDICINE IN RADIOLOGY AND IMAGING.

© 2021

DECLARATION

Declaration by the Candidate

I declare that this thesis is my original work and has not been presented for a degree or any academic credit to any other University or examining body. No part should be reproduced without prior permission from the author or the University.

TITUS NDUGIRE KARIUKI

SM/PGR/01/16

Signature ……………………………………. Date ……………………

Declaration by Supervisors:

This thesis has been submitted for examination with our approval as University supervisors.

Dr. Loice Sitienei,

Lecturer, Radiology, and Imaging

Signature ……………………………………. Date ……………………

Prof Onditi Elias,

Associate Professor, Radiology, and Imaging

Signature ……………………………………. Date ……………………

DEDICATION

I dedicate this work to my dear family members for their emotional support and encouragement during the entire period I was working on it.

ACKNOWLEDGEMENT

ABBREVIATIONS

CECT   Contrast enhanced Computerized Tomography scan

CT   Computerized Tomography

DCF   Deep Cervical Fascia

ENT   Ears, Nose and Throat

IHN   Infrahyoid neck

IREC   Institutional Research and Ethics Committee

KNH   Kenyatta National Hospital

MRI   Magnetic Resonance Imaging

MTRH   Moi Teaching and Referral Hospital

PVS   Paravertebral Space

SHN   Suprahyoid Neck

SPSS   Statistical Package for Social Sciences

US   Ultrasound

TABLE OF CONTENTS

LIST OF TABLES

LIST OF FIGURES

ABSTRACT

Introduction: The neck is divided into two main portions; Suprahyoid Neck (SHN) and Infrahyoid Neck (IHN), each being sub-divided into various neck spaces. These spaces can be affected by congenital anomalies, infection, inflammations, neoplasms, vascular anomalies, and traumatic conditions. Establishing the location of a mass and the space of origin are invaluable steps in developing a differential diagnosis. The use of Computed Tomography (CT) can offer key information for better management of the patients with SHN masses. However, there is a paucity of data regarding its use in Sub-Saharan Africa (SSA). Pathologies of the neck region account for a sizeable proportion of the Ears, Nose and Throat (ENT) admissions in Kenya, with CT imaging done, and the results confirmed with Magnetic resonance imaging (MRI) or histopathological examination. However, in some of these cases, such confirmation is unnecessary if CT can reliably provide the needed diagnosis. But such practices are hindered by lack of data on the agreement between CT and histopathology.

Objectives: The study sought to evaluate the types of neck masses of SHN observed on CT scan at Moi Teaching and Referral Hospital, assess their anatomical site, and compare CT diagnosis to histopathological examination results.

Methods: Cross-sectional descriptive study was done among patients with SHN masses. Census was used with all the 123 patients with SHN masses presenting at the MTRH Radiology Department for the one-year study period, meeting the inclusion criteria included. CT imaging was done, and the images evaluated for size, location, contour, calcification, type of enhancement, necrosis, and fat planes with the adjoining structures, and other supplementary CT findings. For those where histopathology confirmation was done, histopathology results were abstracted. Descriptive analysis was used with mean and standard deviation used for continuous variables like age, while frequency and percentages were used for categorical variables. The differences in proportions and absolute numbers were used to compare CT and histological findings. The results are presented in the form of tables, CT images, and prose form.

Results: Of the 123 patients, 80 (65.0%) were male. The mean age was 44.6 ±16.6 (SD) years. Of the 123 SHN masses, 38 (30.9%) were in the Pharyngeal Mucosal space, 26 (21.1%) parotid space, 13 (10.6%) retropharyngeal space, 13 (10.6%) post-styloid parapharyngeal space, 12 (9.8%) Masticator space, 7 (5.7%) Prestyloid parapharyngeal space, 7 (5.7%) prevertebral space, and one sublingual space. Among them, (55; 44.7%) were malignant, 27 (22.0%) benign, 25 (20.3%) infectious, 7 (5.7%) inflammatory, 6 (4.9%) congenital and 3 (2.4%) traumatic. Most, (60; 48.8%) had heterogeneous enhancement, 28 (22.8%) rim enhancement, and 22 (13.0%) homogenous enhancement. A total of 108 cases had histopathology examination done. There was agreement between CT and histopathology results in 99 (91.7%) cases.

Conclusion: Malignant masses were observed to be the common etiologies in the suprahyoid neck spaces. CT findings showed high agreement with those of histopathological examination, hence an indicator that CT can be reliably used in most SHN masses' diagnosis. However, some cases necessitate further histopathological evaluation to provide more information where it is difficult to diagnose on CT.

Recommendation: In evaluating the SHN masses, radiologists need to pay attention to the type of enhancement, margins, and presence of necrosis, key features that can aid in CT diagnosis. Multicenter and larger studies are needed to provide more evidence on the reliability, sensitivity and specificity of CT in the diagnosis of SHN masses.

CHAPTER ONE: INTRODUCTION

1.1 Background information

The neck is a transitional region that is located between the thorax and the clavicles below and the base of the cranium above (Rea, 2016). The neck is divided by the sternocleidomastoid muscle into two triangles, namely the anterior and posterior triangles, which provide a framework for the anatomical subdivision of the contents of the neck (Rea, 2016; Stathakios & Carron, 2020). Generally, these triangles of the neck are limited by 4 boundaries namely; superior, inferior, anterior and posterior (Rea, 2016). The anterior triangle is further subdivided into 4 sub-triangles; the submandibular and submental triangles which are the superior divisions and while the muscular and carotid triangles constitute the inferior divisions(Al-Missri & Al Khalili, 2020; Stathakios & Carron, 2020).

The submental triangle, also referred to as the suprahyoid triangle, is demarcated by the anterior belly of the digastric muscle , the midline of the neck and the hyoid bone (Al-Missri & Al Khalili, 2020). The hyoid is a U-shaped bone located at the front of the neck and the tongue's root, provides an attachment to a variety of muscles and ligaments that connect it to the cranium, mandible, tongue, larynx, pharynx, sternum and shoulder girdle (AlJulaih & Menezes, 2020; White & Folkens, 2005). Further, the hyoid bone anchors the suprahyoid and infrahyoid muscles hence subdividing the anterior triangle into the suprahyoid and infrahyoid neck spaces(Aiken & Shatzkes, 2020).

The suprahyoid neck spaces consist of the skull base area to the hyoid bone, excluding the oral cavity, paranasal sinuses, and the orbits(Hodler et al., 2020). Each of these portions is further divided into various neck spaces by cervical fascia. The three sheets of the deep cervical fascia, superficial, middle, and deep layers, split the

suprahyoid part of the neck into distinct spaces that are valuable anatomic markers for evaluating pathological alterations and their spread(Hodler et al., 2020).A pictorial illustration of the suprahyoid neck spaces is shown in figure 1.1 below.
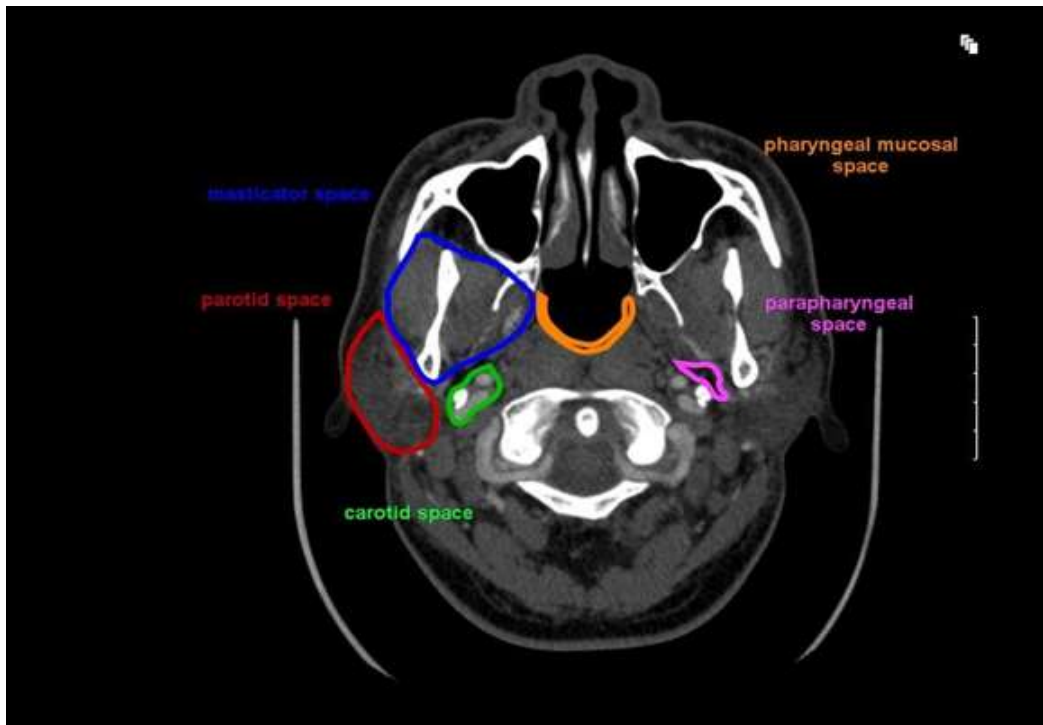
Figure 1.1: Spaces of the suprahyoid neck
Adapted from: Radiologykey.com

1.1.1 Spaces of the suprahyoid head, neck, and fascia

The two main fascial layers of the suprahyoid neck are the superficial cervical fascia and the deep cervical fascia (DCF). The superficial cervical fascia consists of the subcutaneous tissues of the head and neck. The DCF consists of the superficial, middle, and deep layer. The middle layer (visceral or pharyngo-mucosal) encloses the pharynx, which includes the oropharynx and the nasopharynx. The deep layer (paravertebral) is posterior to the visceral fascia and defines the contents of the paravertebral space (PVS) (Aiken and Shatzkes 2020). The suprahyoid neck region spaces are comprised of parotid space, retropharyngeal space, pharyngeal mucosal space, masticator space, prestyloid parapharyngeal space, post-styloid parapharyngeal space or carotid space, and prevertebral space(Aiken & Shatzkes, 2020).

1.1.2 Parapharyngeal space

Parapharyngeal space (PPS) is lateral to the pharynx and is crescent shaped symmetrically. It runs from the base of the skull to the mandible angle and it is laterally enclosed by fascia layer which separates it from the pharyngeal space and masticator space. On the posterior and medial side, it is enclosed by prevertebral and buccopharyngeal fascia. PPS does not have a fascial barrier on the anterior side and is continuous with the sublingual and submandibular spaces(Gamss et al., 2015).

The PPS mainly consist of fat which is easily distinguished on CT and MRI imaging from other types of tissues. Due to this feature of PPS, it helps in the confirmation of the adjacent pathology origin as the PPS is shifted to specific directions by the surrounding mass lesions which plays the role of the indicator of the lesions origin(Gamss et al., 2015). Masses whose primary space of origin is PPS are rare (Shahab et al., 2005).

1.1.3 Masticator space

The masticators space is positioned lateral to the PPS and is the largest SHN space. It is divided into two portions which include the infrazygomatic and the suprazygomatic portions. It extends superiorly to the base of the skull, touching the foramen spinosum and foramen ovale, while it ends inferiorly on the margin of the posterior mandible body. Imaging plays a critical role in circumventing the challenges faces in clinical evaluation of the masticator space (Gamss et al., 2015). Odontogenic infections are common in this space manifesting as abscesses, myositis and cellulitis(Schuknecht et al., 2008). Other common pathologies in this space are the vascular lesions including vascular malformations and hemangiomas (Fernandes et al., 2013)

1.1.4 Pharyngeal Mucosal Space

Pharyngeal mucosal space is divided into oropharyngeal, hypopharyngeal and nasopharyngeal segments. It covers the length of the pharyngeal mucosal surface. It does not have a fascia along its surface. It extends to the hypopharynx inferiorly. The common malignant masses in this space include oropharyngeal and nasopharyngeal carcinoma, salivary glands carcinoma and non-Hodgkin lymphoma. Musculo-skeleton tumors including Chordoma and Rhabdomyosarcoma have been reported. Infections in this space include peritonsillar or tonsillar abscess (Gamss et al., 2015)

1.1.5 Parotid space

This is the space containing the parotid glad and has a fascia which cannot be separated from the gland (Peter M. Som and Hugh D. Curtin, 2011). The parotid gland is divided into two lobes; superficial lobe and deep lobe which are separated by the facial nerve plane (Jacob, 2008). With the imaging identification of the facial nerve being problematic, the retromandibular vein located adjacent to it is mostly used on cross-sectional imaging as a landmark. Imaging might not be the final diagnosis in the parotid space, and core biopsy may be carried out as a confirmatory test for masses in this region(Gamss et al., 2015).

Majority of tumors in the parotid space are benign in nature with pleomorphic adenoma being the most common type(Alvi et al., 2020; Freling et al., 1992) and oncocytoma being the among the least common type (Patel et al., 2011). On the contrary, malignant lesions such as adenoid cystic carcinoma and mucoepidermoid carcinoma have been reported with the latter being the mostly observed type (Maroldi et al., 2008)

1.1.6 Carotid space

This space, also called the carotid sheath, covers both the infrahyoid and the suprahyoid neck. It is found on the styloid process's posterior side, medial to parotid glands, anterior to the prevertebral space, and lateral to the retropharyngeal space(Chengazi & Bhatt, 2019). Pathology associated with this space includes an aneurysm and arteritis linked to the carotid artery, Masses observed in this space include paragangliomas and neurogenic tumors (Gamss et al., 2015).

Space occupying lesions originating in any of these spaces will initially expand the respective space and distort the neighbouring spaces and vessels and structures within the space, which offers the evidence regarding its place of origin(Gamss et al., 2015).A mass centered within the carotid space will displace the parapharyngeal fat/space anteromedial (Gervasio et al., 2011).

In addition, these spaces can be affected by various pathological conditions ranging from congenital anomalies, infection, inflammations, neoplasms, and traumatic conditions. The deep cervical fascia governs the spread of these diseases across these spaces(Borner et al., 2016). Neck masses can be grouped into two types: Nodal masses and Non-nodal masses, both of which can appear as benign or malignant lesions(John R. Haaga & Daniel T. Boll, 2017)

Establishing the location of a mass and identifying the space of origin are invaluable initial steps in developing a differential diagnosis(Patel et al., 2011). Utilization of the three layers of the deep cervical fascia to delineate multiple compartments of the suprahyoid and infrahyoid neck is the current paradigm and allows segmentation of pathology into well-defined facially enclosed spaces. Thereafter, the relationship to the surrounding structures and spaces can be evaluated. A differential diagnosis can

be generated based upon the unique anatomic contents of each space(Gamss et al., 2015).

Imaging is usually carried out to confirm the clinical diagnosis and the extent of the anatomical involvement before treatment is initiated(Balogh et al., 2015). Imaging of the neck has been a challenge to radiologists such that a very close and compact arrangement of vital structures, coupled with complex deposition of Deep Cervical Fascia (DCF) make neck imaging difficult (Forghani, 2015).

A neck mass can be a diagnostic challenge in patients of any age and is commonly evaluated with computed tomography (CT), Magnetic Resonance Imaging (MRI) or Ultrasound (US). Ultrasound, CT, and MRI can all be used in non-invasive assessment of neck lesions(Brown & Harave, 2016; Pynnonen et al., 2017). While ultrasound can provide important information about superficial lesions like those affecting the thyroid and neck vessels, it has got limited spatial resolution and is subject to inter-observer variations as well as poor characterization of lesions in deep spaces of the neck (Galli et al., 2010). MRI is extremely useful in assessment of neck lesions due to its excellent soft tissue delineation and multiplanar imaging capabilities but it is limited by its unsuitability in claustrophobic patients, and individuals with certain (para-magnetic) devices like pacemakers and cochlear implants. Moreover its availability is not uniform and cost is also prohibitive(Shrestha et al., 2011).

CT offers superb distinction of fat from other tissues and is undoubtedly better than MRI to assess bone and calcifications. Additionally, CT is less susceptible to motion artifacts, has a better temporal resolution, and therefore has better compliance with claustrophobic patients as compared to MRI, and can also be done in patients with MRI incompatible devices. Brilliant 3-dimensional imaging is achievable using

volume rendering, maximum intensity projection, and shaded surface display methods, enabling the surgeon to comprehend the lesion's anatomical extent and its relationship to adjacent structures in a much better way (Forghani, 2015).

Before the advent of cross-sectional imaging, radiologists were of limited help in diagnosing neck masses, especially those involving the deep spaces of SHN. The traditional concept of neck anatomy described as various triangles is of little help in cross-sectional imaging, which relies solely on the spatial concept of neck anatomy described in various neck spaces (Shetty et al., 2015).

CT effectively demonstrates these spaces and helps in the characterization of the pathological process. It also helps assess the spread of pathology to contiguous spaces and provides information about regional lymph nodes and vascular anatomy. CT is an invaluable tool in staging head and neck cancers and pre-operative assessment of respectability (Sekine et al., 2017). In addition, use of CT can provide the clinician with critical information for better management of the patients with SHN masses(Kaur et al., 2017) .

The introduction of spiral CT was an essential milestone in the history of neck imaging. Spiral CT rapidly gained acceptance for neck imaging, and today it is the ''gold standard'' for neck imaging. Spiral or helical CT refers to volume acquisition CT, which involves the simultaneous patient translation at a constant rate through the gantry during continuous rotation of source-detector assembly(Semnic et al., 2000).Notable advances in CT have occurred over the years with tremendous impact on clinical practice, including the development of the extreme multidetector CT, iterative reconstruction algorithms, cone-beam CT, dual-energy CT, and phase-contrast CT(Ginat & Gupta, 2014). The MDCT enables visualization of small cortical

bone erosions(Vidiri et al., 2010) while MDCT enables determining the size of solid tumors and monitoring their response during therapy accurately (Ginat & Gupta, 2014)

Positron emission tomography (PET) is an imaging technique that can map functional and metabolic activity before structural changes have taken place. PET scanning using [2- ^{18}F]fluoro-2-deoxy-d-glucose (^{18}FDG) can differentiate malignant from normal tissue based on enhanced glycolysis by tumour cells can thus identify tumour in normal-sized lymph nodes, differentiate sinus malignancy from secretions and fibrosis from tumour(Kropotov, 2016). PET appears to be the best imaging method for assessing recurrent tumours, although there are problems with false positives due to inflammation(Kresnik et al., 2001). A further advantage of PET is the ability to perform whole-body scanning to identify synchronous primary tumours, distant metastases and identify the site of the primary in patients who present with cervical node metastases(Kresnik et al., 2001). However, PET has a limited spatial resolution compared to either computed tomography (CT) or magnetic resonance imaging (MRI)(Vaquero & Kinahan, 2015). This deficiency of PET has been overcome by the development of combined PET-CT whereby the CT scan is used to generate the transmission map, with a consequent decrease in overall acquisition time and provide anatomic co-registration. 18-FDG (350 MBq) is injected, and after a wait of approximately one hour for the tracer to be taken up by the tissues, the images are acquired from the vertex to the pelvis(Cazzato et al., 2018). Standardized uptake values (SUVs) can be calculated (SUV = activity in the region of interest (ROI)/volume of ROI/injected activity/weight of the patient) and can be corrected for partial volume effect. Patients are instructed to remain silent to limit physiologic uptake in the vocal cords(Rankin, 2006).

The neck has a complex anatomy where many critical anatomic structures are compartmentalized into a small space. The traditional classification of the suprahyoid head and neck into nasopharynx, oropharynx and hypopharynx is useful in the evaluation of superficial mucosal lesions but is much less helpful in localizing deep-seated head and neck lesions. Clinicians divide the superficial structures of the neck into anterior and posterior triangles using superficial musculature as landmarks. Anatomists pioneered the work on fascial anatomy and spaces but it was with the advent of cross-sectional imaging that clinicians, surgeons and radiologists adopted the spatial organization of the head and neck into fascial compartments. The basis for dividing the neck into spaces and compartments is the arrangement of the superficial and deep layers of the cervical fascia. This concept can be used to formulate differential diagnosis, determine the extent of disease and facilitate surgical and therapy planning.

1.1.7 Normal Radiological Anatomy and Disease Patterns of Suprahyoid Neck

The clinically used scheme on fascial anatomy and spaces used by the radiologists is based on the arrangement of the two layers of cervical fascia in the suprahyoid neck (SHN) and infrahyoid neck (IHN).The superficial fascia of the neck is composed of subcutaneous fat with the platysma muscle embedded in its deep portion. It encloses the subcutaneous veins, subcutaneous nerves and lymph nodes lie within this space. The superficial fascia encircles the deep cervical fascia (DCF), which contains the major structures of the neck. The DCF is divided into three layers:

1. Superficial or investing layer

2. Visceral or pretracheal layer

3. Deep layer of DCF or prevertebral fascia.

1.1.8 Superficial or Investing Layer

The superficial or investing layer forms a complete collar around the neck and envelops the sternocleidomastoid, trapezius and attaches to the skull base, mandible, hyoid, clavicle, sternum and scapula. The two halves of the fascia attach posteriorly to the ligament nuchae and cervical spinous process. The superficial layer of DCF divides to form the capsules of the submandibular and parotid glands. The spaces included are: masticator space (MS), parotid space (PS), submandibular space (SMS), sublingual space and suprasternal space of burns.

Masticator Space

Masticator space consists of the muscles of mastication which are the medial and lateral pterygoid muscles, masseter and temporalis. The superficial layer of DCF splits to enclose the muscles of mastication and forms the borders of this space. Lesions in the MS typically include nerve sheath tumors, lipomas, mandibular and soft-tissue sarcomas, dental tumors cysts abscesses and osteomyelitis. Vascular lesions, such as hemangiomas, lymphangiomas and rarely pseudo aneurysm, may arise in this space. In children rhabdomyosarcoma may also arise in this space.

Parotid Space

Parotid space is formed as the investing fascia splits between the angles of mandible to enclose the gland forming its capsule. The parotid gland is divided into superficial and deep lobes by the plane of the facial nerve, which lies lateral to the retromandibular vein. The contents of this space are the parotid gland, facial nerve, retromandibular vein, external carotid artery (ECA) and lymph nodes. Evaluation of a mass within the parotid region begins with determination of the lesion as intraparotid or extraparotid. Lesions are considered intraparotid if 50% or greater of the

circumference is surrounded by parotid tissue. Intraparotid masses displace the parapharyngeal fat medially and widen the stylomandibular tunnel. Large lesions of the deep parotid may be difficult to distinguish from primary parapharyngeal mass. Identification of a fat plane between the lesion and the parotid indicates a parapharyngeal space (PPS) site of origin whereas direct continuity of the mass to the gland indicates deep lobe parotid origin. Lesions in the PS include benign tumors, such as pleomorphic adenomas, Warthin's tumors and less commonly, malignant tumors. The parotid gland may be involved by inflammatory pathology. In children 50% of parotid lesions are hemangiomas. Other lesions occurring include calculi, lymph epithelial lesions associated with acquired immunodeficiency syndrome (AIDS), lipomas, first branchial cleft cysts and rarely schwannomas.

Submandibular Space

The SMS is located below the mandible inferior to the mylohyoid muscle while the sublingual space is located above the mylohyoid muscle. The posterior aspect of the mylohyoid muscle is not attached to any bony structure and there is a direct communication between the SMSs with the posterior aspect of the sublingual space. The contents of the SMS are the anterior belly of digastric muscle, superficial portion of the submandibular gland, submandibular and submental lymph nodes, facial artery and vein, inferior loop of hypoglossal nerve and fat. The sublingual space is a tea cup-shaped space that is contained within the mylohyoid muscle. The contents are the anterior extension of the hypoglossal muscle, hypoglossal nerve, lingual artery and vein, sublingual gland and ducts, deep portion of submandibular gland and lymph nodes. Congenital lesions, such as branchial cleft cysts, cystic hygromas, dermoids, epidermoids and thyroglossal duct cysts, may occur in the SMS. Abscesses and inflammation may occur. Tumors of the submandibular gland, such as pleomorphic

adenomas, mucoepidermoid cancers and adenocystic carcinomas, present as soft tissue masses within the gland. Calculi commonly occur in the duct. **Visceral or Pretracheal Layer**

The middle layer of DCF is also known as the visceral or pretracheal layer. It extends from the hyoid bone anteriorly to the pericardium and continues in the SHN as the buccopharyngeal fascia.4 In the SHN the buccopharyngeal fascia encloses the pharynx which includes the nasopharynx and oropharynx. The middle layer envelops the anterior infrahyoid strap muscles and merges with the superficial layer. A portion of the middle layer splits to enclose the contents of the visceral space (VS) in the IHN. The VS contains the major organs of the neck including the trachea, esophagus, larynx, thyroid and parathyroid glands. The fascia splits anteriorly to enclose the sternohyoid and sternothyroid muscles and the posterior split encapsulates the thyroid gland. The spaces included are: pharyngeal mucosal space (PMS), retropharyngeal space (RPS), PPS and buccal space (BS).

Pharyngeal Mucosal Space

Pharyngeal mucosal space is the area of the nasopharynx and oropharynx on the inner side of the buccopharyngeal fascia. The buccopharyngeal fascia separate the PMS from PPS laterally and RPS posteriorly. Therefore, the PMS is composed of five layers, i.e.

(1) Mucous membrane,

(2) Submucosa,

 (3) Dense pharyngobasilar fascia,

(4) Constrictor muscles of pharynx and

(5) Thin buccopharyngeal fascia.

Anteriorly the nasal cavities open into it through the oval posterior choanae. Along the lateral nasopharyngeal wall are two recesses and one protrusion. The recesses are the Eustachian tube orifice and the lateral pharyngeal recess (fossa of Rosen Müller). The protrusion is the cartilaginous portion of Eustachian tube (torus tubarius). The superior portion of the nasopharynx is lined by pseudostratified ciliated columnar epithelium which changes to stratified epithelium inferiorly. Beneath the mucosa and submucosa lies a tissue space containing the muscles that coordinate nasopharyngeal and palatal functions. The major contents include mucosa of pharynx, lymphoid tissue, adenoids and minor salivary gland. The most common malignant lesion of the PMS is non-Hodgkin's lymphoma (NHL), rhabdomyosarcomas and tumors of the minor salivary glands.

Parapharyngeal Space

Parapharyngeal space is an anatomic recess shaped like an inverted pyramid with its base towards the skull and its apex at the greater cornu of the thyroid. The PPS has been divided by some authors (Lewin 1995) into two compartments: the anterior prestyloid compartment which is filled with fat and the posterior post styloid compartment which contains the carotid sheath. However, majority consider the retro styloid compartment as a separate space known as the carotid space (CS) (Hansberger and Osborn).

The PPS is separated from the PMS medially by the buccopharyngeal fascia, laterally from the MS by a layer of investing fascia covering the medial aspect of medial pterygoid muscle and the deep lobe of the parotid gland. Posteriorly it is separated from the prevertebral space (PVS) by the prevertebral fascia. The PPS extends from the skull base to the SMS inferiorly and contains mainly fat. The pharyngeal venous

plexus, the mandibular nerve, the internal mammary artery and the ascending pharyngeal artery are contained within the fat. The other components of PPS are lymph nodes and ectopic salivary gland rests. The importance of the PPS is its central location and the relationship to the other spaces of the neck. The boundaries of PPS are formed by fascial borders of surrounding spaces instead of its own layer of fascia. Primary PPS masses typically displace the lateral wall of them medially, the deep lobe of parotid laterally and contents of carotid sheath posteriorly. Lesions in the space include Schwannomas, benign salivary lesions, lipomas, atypical branchial cleft cysts metastases and lesions spreading from adjacent compartment.

Buccal Space

Buccal space has not received much attention in the radiological literature. It is bordered medially by the buccinators muscle and maxillary alveolar ridge and posterolateral by the MS. Anteriorly it is separated from the subcutaneous tissue by the muscles of facial expression and inferiorly it blends with the SMS. The space contains fat, minor salivary gland tissue, parotid duct, lymph nodes, facial vein, facial and buccal artery, buccal branch of facial nerve and division of the mandibular nerve. Primary lesions are uncommon and include cysts, lipomas and hemangiomas. A dilated parotid duct may be seen due to calculus at the Stensen's duct orifice. The most common lesion in the BS is due to infiltration from buccal squamous cell carcinoma (SCC).

Retropharyngeal Space

Retropharyngeal space is located behind the pharynx anterior to the prevertebral fascia and extends from the skull base up to T4 level. Contents of the suprahyoid RPS are nodes and fat, while the infrahyoid RPS contains only fat. The nodes are arranged into two groups, i.e. the median group and lateral nodes of Rouvière.

1.1..9 Deep Layer of Deep Cervical Fascia or Prevertebral Fascia

The deep layer of deep cervical fascia (DCF) or prevertebral fascia extends from the skull base to the third thoracic vertebra where it fuses with the anterior longitudinal ligament in the posterior mediastinum. The deep layer encircles the vertebrae, paravertebral and paraspinal muscles, vertebral artery and vein, phrenic nerve and trunks of the brachial plexus. The vertebrae are completely enclosed by this layer which attaches firmly to the transverse processes dividing the space into an anterior prevertebral and posterior paraspinal portion .Anteriorly the deep layer splits into two portions. The more anterior portion forms the posterolateral walls of the RPS and contributes to the carotid sheath formation. The more posterior prevertebral portion extends from the skull base to the coccyx. The potential space between the anterolateral alar slip and the posterior prevertebral portion is the danger space (DS). The spaces included extend through the SHN and IHN. These are: CS, RPS, DS, PVS and the posterior cervical space. Within the IHN the three layers of DCF form two additional spaces: VS and the anterior cervical space.

Carotid Space

Carotid space is enclosed by the three layers of DCF as the carotid sheath. This space extends from the skull base to the superior mediastinum and has suprahyoid and infrahyoid components. The suprahyoid CS is also known as the post styloid PPS. Some authors refer to the CS as the carotid sheath. Within the sheath the carotid artery

lies medial to the internal jugular vein (IJV) which becomes anterior to the artery in the lower neck. The vagus nerve lies posterior to the vessels while the sympathetic trunk may be either posterior to the vessels or lie embedded in the sheath wall. The deep cervical chain of lymph nodes abuts the carotid sheath within the CS. Clinicians subdivide the CS into nasopharyngeal, oropharyngeal, cervical and mediastinal segments. The nasopharyngeal CS is also referred to as the retro styloid compartment of PPS. Abnormalities in the CS often show features suggesting their histological diagnosis. These lesions may compress the PPS anteriorly, displace the parotid gland laterally and characteristically display the vessels of the carotid sheath and encroach on the fat of the posterior cervical space in an anterior to posterior directions. A mass in the nasopharyngeal CS displaces the PPS fat and there is an anterolateral movement of the styloid process. A mass in the posterior portion of CS, e.g., vagal schwannoma, neurofibroma and paraganglioma causes draping of the internal carotid artery (ICA) over its anterior aspect. Once pathology is localized to the CS the goal of imaging is to establish the vascular/avascular nature of the mass and assess the relationship of the vascular mass to the vessels of CS. The common pathology of the CS is pseudo tumors, inflammatory lesions, vascular pathology, benign and malignant tumors. There are four distinct spaces between the pharynx and the vertebral bodies from anterior to posterior. They are:

(1) VS,

(2) True RPS,

(3) DS and

(4) PVS.

These spaces allow the spread of disease and infection along the neck and torso. Retropharyngeal space, DS and PVS are distinct midline spaces of the extra cranial

head and neck. The RPS and DS are potential spaces posterior to the pharynx bounded by the middle and deep layers of DCF. The anterior boundary of the RPS is formed by the middle layer of DCF, while its posterior and lateral boundaries are formed by the alar portion of the deep layer of DCF. The DS is formed by the splitting of the deep layer into an anterolateral alar slip and a posterior prevertebral portion. Both RPS and DS extend from the skull base to the upper mediastinum where the middle and deep layers of the DCF fuse obliterating the RPS, while the DS continues inferiorly below the termination of the RPS to the level of the diaphragm. The contents of the suprahyoid RPS are fat and lymph nodes, while the infrahyoid RPS contains only fat. The lymph nodes lie on either side of suprahyoid RPS usually on the longus colli muscle between the CS and VS and enlarged nodes displace the PPS anteriorly.

Prevertebral Space

The PVS is a posterior midline space of the SHN and IHN enclosed by the deep layer of DCF which lies posterior to the RPS. It extends from the base of the skull to the level of coccyx. The deep layer of fascia is attached to the transverse processes anteriorly and posteriorly to the spinous processes and ligamentum nuchae thus dividing the PVS into two fascially defined compartments. The anterior compartment is known as the PVS proper which contains the prevertebral and scalene muscle, roots of brachial plexus vertebral bodies and pedicles, phrenic nerve, the vertebral arteries and veins. The posterior compartment is the paraspinal portion which contains the paraspinal musculature, vertebral laminae and spinous processes. Normally RPS and PVS should not exceed 7 mm at C2 for both children and adults. At C6 soft-tissue space should not be more than 14 mm for children and 22 mm for adults. *Inflammatory lesions* represent a significant portion of pathology. Etiologies include

tuberculous spondylitis, pyogenic osteomyelitis and postoperative infections. *Anterior cervical spaces* contain only fat. *Posterior cervical spaces* extend from the skull base to the clavicles and the anterior cervical spaces from the hyoid bone to the clavicle. They lie among all three layers of DCF and have complex fascial boundaries. These fat-filled spaces provide constant landmarks on CT and MR. The contents of posterior cervical space are the spinal accessory nerves and their lingual nerve (LN) chains, dorsal scapular nerves and the transverse cervical vessels. *Tumors arising* in the posterior cervical space may be benign, malignant or neural sheath tumors. *Schwannomas* and neurofibromas arising in the neck are located most commonly in the CS or posterior cervical space. *Lipomas* are encapsulated collections of mature fat cells found predominantly in the posterior cervical space. They are easily identified by their imaging characteristics. *Sarcomas* primarily arise in the posterior cervical space. Liposarcomas are easily identified due to their fatty content while rhabdomyosarcoma, neurofibrosarcoma and fibro sarcoma have no distinct radiological findings and are diagnosed on biopsy.

Normal cervical lymphatics and lymph nodes:

 The cervical lymph nodes are arranged in clusters and chains each with characteristic drainage. Lymph node clusters are named according to the fascial space they occupy while the lymph node chains are named according to the anatomic structures they accompany. The clusters in the neck are submental, submandibular and retropharyngeal while the chains are juxtavisceral, external jugular, internal jugular, spinal accessory and transverse cervical. A normal node is oval with a well-defined border, not greater than 10 mm on transverse diameter except the jugulodigastric and juguloomohyoid nodes which may be as large as 15 mm. Children have larger normal nodes than adults. The submental nodes lie between the anterior bellies of the

digastric muscles, submandibular between the anterior and posterior bellies of digastric separated from the submandibular gland by the anterior facial vein. The submental and submandibular group form surgical level I. The upper jugular group comprising the superior third of the internal jugular chain and superior half of the spinal accessory chain from the skull base superiorly to the carotid bifurcation comprises level II. Level III is the middle internal jugular group extending from the carotid bifurcation or hyoid bone to the cricoid cartilage where the omohyoid muscle crosses the internal jugular chain. Level IV is the lower jugular group extending from the cricoid cartilage to the clavicle. Level V is the posterior group comprising of the inferior half of the spinal accessory chain along with the entire transverse chain. Level VI is formed by the grouping of juxtavisceral anterior cervical and external jugular chains. The juxtavisceral lymph node chain consists of a group of four chains:

(1) Prelaryngeal,

(2) Parathyroid,

(3) Pretracheal and

(4) Para tracheal chains.

The retropharyngeal lymph nodes are divided into media land lateral clusters:

(a) The medial cluster lies behind the nasopharynx at the level of the atlantoaxial junction and

 (b) The lateral cluster lies anterior to the carotid sheath.

These nodes are the deepest node group and are not palpable and excluded from surgical level classification because they are not involved in neck dissection. Ultimately all lymphatics drain from the head and neck into jugular trunks which lie lateral to the internal jugular vein. The left jugular trunk drains into the thoracic duct while the right empties directly into the subclavian vein.

1.1.10 Imaging Techniques

Imaging techniques are useful in assessing clinically occult lesions disease in blind areas, especially in the lateral pharyngeal recess, extra mucosal lesions, uncooperative patients and post treatment assessment. Plain radiographs were once the mainstay of diagnosis. Soft-tissue radiographs of the neck in the lateral position are used to delineate mass lesion but soft-tissue interfaces are often not visualized optimally. Fractures, cervical spine abnormalities and airway compromise are well seen on plain radiographs. Fistulous or sinus tracts are seen on contrast examinations. Tomography and xeroradiography give a better delineation of air-filled structures but superimposition of structures, variation in airway contour pose difficulties in

Interpretation. Ultrasonography (USG) performed with a high frequency linear probe is excellent for visualizing superficial lesions. It differentiates solid from cystic lesions and can evaluate the vessels of the neck. Ultrasound (US) provides a guidance for fine-needle aspiration. Cross-sectional imaging with computed tomography (CT) and magnetic resonance (MR) have greatly extended our capabilities to image this region. The entire head and neck region should be scanned with CT or MR from the skull base to the thoracic inlet. Contrast-enhanced (CE) studies should be done to depict the vascularity of the lesion and opacify the arteries and veins. Spiral techniques allow high-quality three-dimensional (3D) reconstructions which are helpful in evaluating the craniocaudally extent of the lesion. The advent of multidetector CT (MDCT) has revolutionized the imaging of neck spaces. The fast image acquisition of multiline scanners allows dynamic maneuver during the examinations. Such maneuvers include:

Phonation (for a better visualization of laryngeal ventricle),

Modified Valsalva (for a better visualization of the pyriform sinuses, post cricoid region and the gingivobuccal tumors).

A dynamic acquisition of neck mass sections during administration of the bolus of the contrast agent is possible with the newer CT machines.

1.2 Perfusion Computed Tomography

Computed tomography perfusion imaging is a dynamic technique for quantitative assessment of tissue microcirculation and is a noninvasive tool for the evaluation of microcirculatory changes associated with head and neck cancers. Perfusion CT measures tissue blood supply, tissue vascularity and contrast clearance. It is a potential imaging tool to assess tumor activity because every neoplasm is characterized by neovascularity and increased angiogenic activity. MDCT scanners, especially the 64 and 128 row scanners, provide a greater anatomic coverage without table motion and higher temporal resolution compared with previous CT technology. This enables more extensive and accurate evaluation of primary and recurrent head and neck tumors and local lymph node metastases. It allows evaluation of areas with different perfusion patterns, such as viable versus necrotic tissue. CT perfusion analysis is based on continuous recording of X-ray attenuation by a small fast bolus of iodinated-contrast medium over a first target region. The dynamic acquisition lasts for a time covering the first pass of iodinated-contrast medium in the regional vascular bed during which it has an intravascular distribution. Region of interest (ROI) is drawn on the tumor and the ipsilateral common carotid artery or ECA as close as possible to the tumor. Scanning starts 10 seconds after the beginning of iodinated-contrast medium injection and ends 50 seconds thereafter. This allows measurement

of vascular permeability and avoids unnecessary radiation exposure. The following quantitative perfusion parameters are defined: __ Blood flow (BF) __ Blood volume (BV) __ Mean transit time (MTT) __ Permeability surface area product. A significant increase in BF, BV and permeability surface area product along with a significant reduction in MTT have been found in malignant head and neck tumors. It is also seen that SC CA of the upper aero digestive tract with increased BF and BV are more chemo sensitive than those with decreased perfusion parameters. It has been observed that less perfused tumors respond poorly to radiation therapy as a result of their lower oxygen content. CT perfusion is useful in the assessment of disease recurrence after radiation therapy and for the characterization of lymph nodes.

1.2.1 Magnetic Resonance Imaging

While imaging neck spaces, a combined head and neck coil should be used for a comprehensive evaluation of the entire extra cranial head and neck, evaluating all the nodal masses, a second primary neoplasm and perineal tumor spread. In addition to the conventional CE-MR, axial diffusion weighted imaging (DWI) may also be performed. Neoplasms are associated with alterations in water diffusivity and microcirculation of the node. DWIs can be obtained with a single shot echo planar imaging (EPI) sequence by the same coil and quantification of the diffusion abnormalities is calculated as apparent diffusion coefficient (ADC).

Diffusion-weighted MRI of Nodes

Metastatic nodes show a restricted pattern of diffusion, i.e. increasing hyper intensity with increasing "B" values corresponding to low ADC values. Necrotic areas within the nodes show mixed signal intensity (SI) at different "B" values and high SI on the ADC maps are essential to show the necrotic areas and differentiate malignant from

benign nodes. The ADC criterion is the strongest independent predictor of the presence of metastasis as ADC values of malignant lymph nodes are significantly lower than benign lymph nodes. Quantitative DWI enables the detection of sub centimeter nodal metastases although micro metastases smaller than 4mm can still be missed. Quantitative DWI has a high negative predictive values for the exclusion of metastatic disease.

Perfusion MR Imaging

Similar to perfusion CT, dynamic MRI offers the potential of visualizing the tumor vascularity. EPI or a VIBE (volumetric interpolated breath-hold examination) sequence are used and mean SI versus time curves are plotted. Parameters, such as peak time (in seconds), peak enhancement (percent baseline) and washout slope, estimate can be obtained.

Dynamic Contrast-enhanced CT and MRI of the Nodes

Dynamic contrast-enhanced CT (CECT) and MRI are helpful to distinguish tumor involved from noninvolved lymph nodes in, e.g., SCCa of the head and neck. Metastatic nodes have a longer time to peak, reduced maximum slope and a slower washout.

1.2.2 Proton MR Spectroscopy

Another promising MRI technique is proton magnetic resonance spectroscopy (MRS) wherein data can be acquired on the same scanner and with the same coils. Single voxel spin echo sequence (SVS) can be used and it allows detection of the choline signal which is higher in neoplastic tissue. Metastatic nodal disease has a characteristic spectrum and shows a higher choline concentration due to the neoplastic tissue.

1.2.3 Lymph Node Specific MR-contrast Agents

Tissue-specific imaging techniques, such as ultra-small super paramagnetic iron oxide (USPIO) agent can play a significant role in detecting or excluding nodal metastases. Advantages of these agents over gadolinium-based contrast agents are that they have a long intravascular half-life (> 30hours) and delayed imaging 24–36 hours after administration continues to show localization of USPIO in the lymph nodes. Dextran-coated USPIO accumulates in normal functioning lymph nodes because small iron oxide particles are taken by macrophages in these nodes.16 Because of the magnetic susceptibility effects of iron oxide normal nodes show reduced SI (negative enhancement) on postcontrastT2-weighted (T2W) spin echo (SE) and T2W gradient echo images. Metastatic nodes remain hyper intense because of the reduced phagocytic activity. The role of USPIO imaging in assessing for recurrent nodal disease in the treated neck requires further prospective investigation.

1.2.4 Tumor Recurrence versus Treatment Changes: Positron-emission Tomography

New imaging techniques outside of cross-sectional imaging have focused on the physiological properties of tumors and tissue characterization rather than anatomic detail. Positron-emission tomography (PET) using 2-deoxy-2-(18F) flour-D-glucose (18F-FDG) relies on the metabolic activity of neoplasms relative to the adjacent tissues in positively identifying the presence of tumor. PET imaging may be useful in the detection of known primary cancers, in guiding endoscopic biopsies, in evaluating recurrent tumors and indistinguishing recurrent neoplasm from radiation changes. One of the potential pitfalls of CT and magnetic resonance imaging (MRI) is their inability to distinguish treatment changes from recurrent tumor. In general, recurrent neoplasms show significant uptake of 18F-FDG compared with fibrotic tissue and radiation necrosis thus allowing the distinction.

1.3 Nodal Neck Masses

Nodal neck masses represent one of the most common and important masses of the neck. The first step in assessing the neck for metastatic disease is knowledge of nodal classification, namely the anatomic level of pathologic nodes

Staging

Nodal staging is concerned with the presence or absence of nodal disease, nodal size and assessment of the involved nodes. The American Joint Committee on Cancer (AJCC) and the International Union against Cancer (UICC) developed in 1987 a common staging system intended to overcome the pitfalls of the subjective palpation of the nodes.

Imaging Characteristics: Cross-sectional Imaging

In the assessment of regional nodal metastases in patients with head and neck cancer, the radiologist must identify if pathologic nodes are ipsilateral, contralateral, or bilateral. Pathologic lymph nodes are established either by size (enlargement) or the presence of abnormal nodal architecture. In addition, the presence of extracapsular spread of tumor, carotid encasement and fixation of the tumor to the skull base or PVS should be evaluated because these features of cancerous nodes affect prognosis and management.

Lymph Node Size and Contour

The initial criteria of level I and II nodes larger than 1.5cm at their maximum diameter and nodes elsewhere (>1cm for nodal malignancy) has been found to be somewhat inaccurate. Brekel and colleagues suggested an axial diameter of 8–9 mm in level II and 7–8 mm elsewhere for metastatic nodes. Based on the observation that metastatic nodes tend to be spherical whereas non metastatic nodes tend to be oblong

ratio of the maximum longitudinal length to the maximum axial length is taken. The ratio exceeds the value of 2 in normal hyperplastic nodes and is less than 2 in metastatic nodes. Nodal size alone cannot be used as a reliable criterion for diagnosis of metastasis.

Nodal Necrosis

The detection of nodal necrosis in untreated patients seems to be the most reliable sign of metastatic disease. The CT appearance of nodal necrosis is a low-attenuated area while the MRI appearance is of liquefaction necrosis and a hyper intense area inside the node. The frequency of necrosis in a metastatic lymph node increases with lymph node size. Necrosis is seen in 10–30% of metastatic nodes smaller than1 cm and 56–63% in nodes larger than 1.5 cm. Overall a distorted internal architecture is the pathognomonic feature for metastatic nodes from head and neck cancers.

Nodal Calcification

Cervical lymph node calcification is rare and seen in about 1% of lymph nodes, most often in papillary thyroid cancer. It is occasionally seen in metastatic mucinous adeno-CA, treated lymphoma and granulomatous disease.

Extracapsular Neoplastic Spread

Indistinct nodal margins, irregular nodal enhancement or infiltration in the adjacent fat or muscle are features suggestive of extracapsular neoplastic spread. Another grave prognostic finding of metastatic nodal disease includes an arterial invasion of the adjacent carotid artery. Preoperative identification of carotid encasement is important for treatment planning. The presence of tumor around the ICA by a circumference of less than 180° normally indicates the absence of invasion whereas tumor that encases the carotid artery by greater than 270° is usually indicative of

invasion. Using CT, MR or US carotid involvement of 270° or more is predicted arterial wall invasion with a sensitivity of92–100% and specificity of 88–93%.

Skull Base and Vertebral Invasion;

Identification of tumor extension to the skull base or prevertebral compartment is important because it frequently indicates inoperability. MRI can be used in the assessment of the PVS. The retropharyngeal fat between the tumor and prevertebral musculature can be identified on unenhancedT1W-MR images. The prevertebral longus muscle complex is evaluated for muscle contour, irregular tumor muscle interface, T2 hyper intensity enhancement and loss of the retropharyngeal fat plane. The preservation of fat plane incorrectly indicative of absence of fixation to the prevertebral muscles in 97.5% patients. Occult malignancies presenting with cervical lymphadenopathy pose an especially difficult management problem. Causes for the inability to clinically locate the primary lesion include small size at presentation, inaccessibility to clinical inspection, and predominately deep submucosal pattern of spread and even spontaneous regression of the original pathology. Imaging is useful in identifying the location of the occult primary neoplasm, suggesting a possible biopsy site and assessing the extent of the disease. In patients with metastatic nodes originating from an unknown upper aero digestive tract site and a negative blind biopsy, CT can suggest the primary tumor in almost 25% of cases. Patients with occult SCCa metastatic to level me or level II nodes should undergo imaging of the nasopharynx, oropharynx and hypopharynx. Of occult primary tumors initially presenting with lymphadenopathy, the nasopharynx is the most commonly encountered site. Submandibular lymphadenopathy suggests the tongue and floor of the mouth as primary sites. Upper cervical node involvement should also prompt inspection of the base of the tongue and tonsillar region. Middle and lower internal

jugular node involvement suggests larynx, hypopharynx or thyroid primary sites. Midline and paratracheal nodes may be involved in thyroid, larynx and even lung cancers. Involvement of the supraclavicular nodes may be the result of spread of thoracic and even abdominal malignancies. In the past decade, 18F-FDG single-photon emission computed tomography (SPECT) has yielded promising results as an adjunct to conventional cross-sectional imaging in evaluating the occult malignancy. Lymphoma is the second most common malignancy in the neck and also the most common extra laryngeal malignancy. Hodgkin lymphoma is one of the most common neck malignancies in children. Lymphoma of the neck commonly involves the adenoids, lingual and pharyngeal tonsils (Waldeyer's ring). The cervical lymph nodes, especially the internal jugular and spinal accessory nodes, also usually are involved. Extra nodal sites, such as the thyroid gland, also may harbor malignant disease. On imaging, clusters of round, nonnarcotic nodes are often observed. Large cell lymphoma may cause especially large nonnarcotic lymph nodes. Attenuation and enhancement properties are variable. Necrosis may be seen following therapy. Almost 50% of AIDS patients have neck abnormalities. Homogeneous cervical lymphadenopathy in a young patient with associated nasopharyngeal lymphoid hyperplasia and lymph epithelial parotid lesions should prompt consideration of human immunodeficiency virus (HIV) infection. Of AIDS patients with NHL of the neck, most are severely immunodeficient, exhibit extra nodal disease, have aggressive tumors and respond poorly to treatment. Necrotic nodes in these patients should also prompt evaluation for a primary SCCa or Kaposi sarcoma. Tuberculous lymphadenitis typically affects young patients and may present as a conglomerate mass of necrotic, enhancing and often calcified nodes associated with inflammatory changes in the skin and adjacent fascial planes. Unlike acute suppurative lymphadenitis, tubercular nodes

are usually painless and may even resemble aggressive cancer or lymphoma. Other conditions producing cervical lymphadenopathy include infectious mononucleosis, sarcoidosis, sinus histiocytosis with massive lymphadenopathy and Castleman disease. Newer imaging techniques, such as diffusion-weighted MRI of lymph nodes, dynamic CECT and MRI of nodes, proton MRS and lymph node-specific MR contrast agents can help to differentiate between benign and malignant lymphadenopathy.

1.4 Non-Nodal Neck Masses

A simple approach in evaluating neck lesions is based on the fact that the neck is a symmetric anatomic structure with the right half being a relative mirror image of the left. Majority of lesions can be easily localized to their space of origin. Large masses can be transpatial when distortion of normal anatomy on the involved side can be compared to the corresponding area on the uninvolved side to identify the location of the epicenter of the mass.

1.5 Masses of Developmental Origin

Branchial Cleft Cysts

Branchial cleft anomalies are thought to arise because of incomplete obliteration of a portion of the branchial apparatus. A first branchial cleft cyst arises from the residual embryonic tract which extends from the external auditory canal (EAC) through the parotid gland to the submandibular region. It is of two types: type I is usually preauricular in location and type II is periparotid extending from the EAC to the angle of the mandible the most common and typical location of a branchial cyst is at or immediately inferior to the angle of the mandible (type II). A cystic lesion at the angle of the mandible displacing the sternocleidomastoid posteriorly, carotid artery and jugular vein medially and the submandibular gland anteriorly is characteristic. The

second branchial anomaly may cause fistulas, sinuses or cysts. It can occur anywhere from the tonsillar fossa to the supraclavicular region. Bailey classified second branchial cleft cysts into four types:

(1) Type I is the most superficial and lies along the anterior surface of the sternocleidomastoid muscle just deep to the platysma;

(2) Type II is found along the anterior surface of the sternocleidomastoid muscle, lateral to the CS and posterior to the submandibular gland;

 (3) Type III extends medially between the bifurcation of the ICA and ECA

(4) Type IV is seen in the PMS. Third and fourth branchial cleft cysts are rare. Most third branchial cleft cysts lie posterior to the sternocleidomastoid muscle. Fourth branchial cleft anomalies are usually sinus tracts which arise from the pyriform sinus through the thyrohyoid membrane and descend into the mediastinum.

Ranula

Ranula is a cystic lesion most commonly originating in the sublingual glands. Strictly speaking this is a large, soft mucus containing lesion that occurs in the floor of the mouth and is typically seen in infancy a plunging ranula is the term used for a lesion that has enlarged to pass behind and through the mylohyoid sling. This may be seen in any age group.

Lymphangioma

Cystic hygroma is the most common of lymphangiomas constitutes about 5% of all benign tumors of infancy and childhood. They usually result from blockage of lymphatic channels. In children, the most common location is the posterior cervical space and the oral cavity. They usually present at birth as a painless swelling and most

lesions (90%) occur before the age of 2 years. In adults lymphangiomas are more commonly seen in the sublingual space, SMS and PS. Less commonly these are seen in the axilla, mediastinum, abdominal cavity, retro peritoneum and even the skeleton.

Imaging Features

These lesions are characteristically infiltrative in nature and do not respect fascial planes. They are composed of multiple dilated cystic spaces separated by minimal intervening stroma. On US they appear as a multinodular predominantly cystic mass with septa of variable thickness. Fluid-fluid levels may be seen with layering in the dependent portion of the lesion. On CT these lesions are poorly circumscribed, multiloculated, hypo attenuating masses with a fluid attenuation, which can extend from one space in the neck to another. On MR the most common pattern is that of a mass with low or intermediate SI on T1W images and hyper intense onT2W images. Less frequently the lesion may be hyper intense on T1W images when there is high-lipid content. In case of hemorrhage, fluid-fluid levels may be observed. The insinuation around the normal structures is well demonstrated on MRI and this can make complete surgical removal of the lesion difficult. 10% of cervical cystic hygroma may extend into the mediastinum. Imaging is performed to assess the extent of the lesion and its relationship to the adjacent structures before surgical excision.

Thyroglossal Duct Cyst

The most common congenital neck mass is a thyroglossal duct cyst. It is the remnant of the thyroglossal duct which originates between the foramen cecum at the tongue base and the thyroid bed. Its location is in the midline or paramedian and is closely related to the hyoid bone and maybe suprahyoid or infrahyoid. A low-density cystic midline mass embedded within the strap muscles with a smooth, thin, well-defined

wall is characteristic. Occasionally it can be septated and peripheral rim enhancement may be seen. Increased attenuation and wall enhancement is seen if complicated by infection. The presence of mural nodules or foci of calcification within the cyst would suggest thyroglossal duct Ca.

Dermoid and Epidermoid Cysts

Both dermoid and epidermoid cysts are composed of epithelial elements. On CT fatty internal elements, mixed density fluid and calcification can be found in dermoid cysts whereas epidermoid cysts are of fluid density with little or no complex features. Most cervical dermoid cysts occur in the midline or just off midline and are usually present at birth. In contrast to thyroglossal duct cysts, dermoid cysts typically do not move with swallowing. Epidermoid cysts typically involve the floor of the mouth incorporating the sublingual space, SMS and the root of the tongue.

Tornwaldt's Cyst

It is a congenital midline posterior PMS cyst lined by pharyngeal mucosa. There is focal adhesion of pharyngeal mucosa to the notochord resulting in a nasopharyngeal diverticulum. Peak incidence is 15–30 years and majorities are incidental findings on head MRI. Infection with anaerobic bacteria raises the intracystic pressure, the orifice opens making the patient symptomatic.

Imaging Features

Computed tomography scans shows a well-circumscribed thin-walled midline posterior naso-PMS cyst lodged between the prevertebral muscles. Attenuation of the cyst increases as the protein content increases with infection and may mimic soft-tissue mas on MR the cyst has a T1-SI, which increases from low to high with increasing protein content. The SI is high on T2W images.

1.6 Masses of Inflammatory Origin

The inflammatory lesions vary from cellulitis, an infected retention cyst, a cervical manifestation of a systemic inflammatory disease (like sarcoidosis) or a potentially life threatening deep neck abscess.

Tonsillitis and Peritonsillar Abscess

Acute tonsillitis or adenotonsillitis may be viral or bacterial and is usually self-limiting but severe infection of PMS may result in a tonsillar abscess (Quinsy). The abscess may extend deep into the neck to involve the PPS or lateral part of RPS. Imaging is performed occasionally in complicated tonsillitis to confirm the diagnosis of abscess and determine the extent. Infection of the PPS (prestyloid) space most commonly arises from spread of peritonsillar abscesses, retro tonsillar vein thrombophlebitis, and third molar extractions with injury to the pterygomandibular raphe, penetrating injury to the lateral pharyngeal or extension from the wall, instrumentation, parotid gland, submandibular gland, brachial cleft or PNS and temporal bone infections.

Imaging Features

On noncontract CT scans the inflammatory process appears hypo dense to isodense. On MR images it is hypointense to isointense to the surrounding muscles on T1W and hyper intense on T2W images. Post contrast studies delineate the enhancing rim of the mature abscess that requires drainage.

Acute and Chronic Parotitis

Inflammatory lesions of the parotid gland may be acute or chronic

Acute Parotitis

Acute viral parotitis is often secondary to mumps and may be unilateral or bilateral. On sonography the gland is diffusely enlarged and may have a normal, heterogeneous or hypoechoic textures. Acute bacterial or suppurative parotitis is seen in children under 1 year of age. It is commonly due to *Staphylococcus aureus* and is unilateral. Sonographically the enlarged parotid gland has a heterogeneous echotexture. Discrete hypoechoic nodules may be noted within the substance of the parotid gland representing enlarged intraparotid nodes. Cervical lymphadenopathy may be found. Acute recurrent parotitis is usually seen at 2–5 years of age and episodes tend to diminish near adolescence. The gland may be normal or there may be mild sialectasis and lymphocytic infiltration. On sonography the enlarged parotid gland shows multiple hypoechoic areas measuring 2–4 mm in diameter. These areas due to peripheral sialectasis may persist even when symptoms disappear.

Chronic Parotitis

Chronic parotitis is bilateral in most cases. It may be caused by recurrent bacterial infection, granulomatous diseases, radiation therapy, autoimmune diseases or idiopathic processes. Granulomatous inflammations include tuberculosis, sarcoidosis and cat-scratch disease (Figs 19Aand B). Toxoplasmosis, actinomycosis and fungal diseases may involve the parotid gland. HIV infections may lead to painless parotid involvement and is usually associated with lung disease. Mucosa-associated lymphoid tissue (MALT) lymphoma presents with bilateral parotid swelling in patients with HIV infection. In sarcoidosis, the parotid glands are affected in 10–30% of patients most often bilaterally (80%) (Figs 20A to C). There may be a triad of uveitis, facial nerve paralysis and parotitis seen in Heerfordt's syndrome.

Imaging features:

Sonography and CT scan may be used to image the salivary glands. On sonography two patterns maybe seen:

(1) The most common pattern (70%) consists of multiple hypoechoic or anechoic areas within the parotid without posterior acoustic enhancement; this is due to lymphoid infiltration in an enlarged gland and

(2) The second pattern (30%) consists of large anechoic areas within the parotid replacing most of the gland; these lesions represent lymphoepithelial cysts. Lymph nodes are normally seen in abundance outside the parotid gland and lymph tissue is normally present within the gland. Hence, extra parotid inflammation may involve the intraparotid lymph nodes secondarily. Color Doppler imaging shows these nodes to have an increased vascular flow.

Sialolithiasis

Approximately 80–90% of salivary gland calculi occur in the submandibular gland and only 10% in the parotid gland. They may be intraglandular or intraductal and can be visualized well on sonography. Associated sialectasis may also be well seen on sialography or sonography. Disruption of the duct may lead to mucocele formation. Calculus disease is the most common cause of salivary inflammatory lesions, especially in SMS, owing to the upward secretion of the more mucinous, viscous and alkaline saliva. Patients with calculus disease have painful glands and calculus disease is often associated with fever. CT imaging is preferred to MRI for identifying calculi MRI is useful for detecting mandibular infection (osteomyelitis) and to differentiate between cellulitis/myositis and abscess. It demonstrates an enhancing submandibular gland and offers the advantage of MR Sialography. Fat infiltration or gland size

reduction, compared to the healthy side in MRI may also indicate chronic disease with sialadenitis.

Ludwig's Angina

Ludwig's angina is an acute bacterial cellulitis with phlegmon formation but little or no pus formation involving the floor of the mouth and commonly the SMS. It was first described in 1836 by Von Ludwig. The infection most commonly afflicts patients between 20 years and 50 years of age and is rarely seen in children. The progress of infection may be very rapid within hours leading to respiratory obstruction due to swelling and poster superior displacement of the tongue. The patient has pain, dysphagia, trismus and swelling of the SMS. The infection may also extend to the PPS, RPS and CS if untreated. Rarely spread may occur into the mediastinum.

Ranula

Ranula is an inflammatory lesion of the sublingual space. The lesion is actually a mucous retention cyst that may result from an obstructed sublingual or minor salivary gland or from trauma or retained secretions that may lead to rupture of acini. A ranula may herniate through the mylohyoid muscle into the submandibular or lower PPS and evolve into a plunging ranula. On CT ranulas have high-fluid attenuation, the cyst wall may or may not enhance depending on infection. A plunging ranula has a distinct "tail sign" within the sublingual space with the bulk of the cyst seen in the SMS.

Osteomyelitis

Osteomyelitis of the jaws is an important differential diagnosis in inflammatory masses of the neck. It may develop as a result of odontogenic infection, focal injury after tooth extraction or complicated fracture or may occur in an immunocompromised patient. It may present radiographically as suppurative,

sclerosing or tuberculous lesion and may present with periostitis. Low SI on T1Wimages and high SI on T2W images of the bone marrow is characteristic of the disease. Soft-tissue involvement with edema and abnormal enhancement is also common in osteomyelitis. However, this pattern is also found in osteoradionecrosis in irradiated patients or in bisphosphonate-induced osteonecrosis.

Inflammatory Pathology of the Carotid Space

Carotid space infection is well-contained within the carotid sheath. CS abscess is a surgical emergency as delayed intervention can lead to carotid artery perforation and exsanguination. Enhanced CT or MR demonstrates an enhancing rim around an abscess. On MR T1W images show low signal and a high signal which is seen on T2W images. Inflammations of the deep cervical lymph nodes of the CS maybe reactive when the lymph nodes appear homogeneous and are less than 1.5 cm in diameter. Diffuse enlargement of lymph nodes may be seen in infectious mononucleosis, sarcoidosis and tuberculosis. Regardless of the organism suppurative nodes appear malignant due to their inhomogeneous internalarchitecture. Patients with tuberculosis have extensive adenopathy involving the internal jugular and spinal accessory chains. Nodes are matted and may form conglomerate masses with necrosis and thick indistinct margins. Calcifications may be present. In patients with AIDS diffuse lymphadenopathy maybe present with tonsil enlargement and affected lymph nodes appear homogeneous on CT and MR.

Inflammatory Disease of the Retropharyngeal Space

The palatine tonsils and the nasopharyngeal adenoids are important sites of infection. Spread to the lateral retropharyngeal nodes may result in suppurative lymphadenopathy. The RPS is a potential conduit forth spread of infection from the

neck to the posterior mediastinum. Tubercular infections of the spine may spread from the PVS to the RPS. Direct trauma and iatrogenic causes may also cause infections and inflammations.

Imaging Features

The main aim is to differentiate cellulitis which can be treated medically and an abscess which usually needs surgical intervention. On CT, an abscess appears as an area of low attenuation with peripheral rim enhancement and on MRI it is seen as high SI on T2W images. On CT imaging, abscesses appear as single or multiloculated, low-density masses that conform to fascial spaces. Abscesses demonstrate peripheral rim enhancement. Cutaneous and subcutaneous manifestations of infection include enlargement of adjacent muscles (myositis), thickening of the overlying skin, and obliteration of the fat planes and enhancement with thickening of the fascial planes. Cellulitis can easily spread to adjacent fascial spaces, upward or downward. If a diagnosis of cellulitis is made and the patient shows no response to appropriate antibiotic therapy, a second examination should be performed to ensure that an abscess cavity has not formed.

Inflammatory Lesions of the Prevertebral Space

These represent a significant portion of PVS pathology. Etiologies include tuberculous spondylitis, pyogenic osteomyelitis and postoperative infections.

Imaging Features

Vertebral body involvement is a conclusive sign of PVS involvement. A mass in the PVS proper has its center on the vertebral body or prevertebral muscles and displaces the prevertebral soft tissue. A mass from the paraspinal portion has its center on the paraspinal musculature or posterior elements of the vertebrae and displaces the Para

spinous muscles and posterior cervical space fat outwards away from the spine Therefore, a primary PVS mass typically displaces the RPS and posterior wall of VS anteriorly and the carotid sheath laterally. In tuberculous spondylitis the inflammation is centered at the disk space often associated with partial destruction of the anterior part of the vertebral body. Typically this is associated with large paraspinal, frequently calcified, soft-tissue mass. Pyogenic vertebral body osteomyelitis presents at the disk space with decreased height, subchondral bony erosions and fragmentation of the vertebral body without well-defined margins. Both tubercular and pyogenic infections may extend into the epidural space. *Necrotizing fasciitis* is a rapidly spreading infection throughout the tissue planes of the neck seen mainly in the elderly and immunocompromised. The causative agent's *Streptococcus* and mixed flora. Multiple neck spaces are involved with thickening of the subcutaneous tissues, enhancement of cervical fascia and muscles, fluid and air collections and reactive lymphadenopathy. Complications may lead to sepsis and mediastinitis.

1.7 Masses of Neoplastic Origin

Benign Tumors

Juvenile Nasopharyngeal Angiofibroma

It is the most common benign yet locally invasive no capsulated mesenchymal tumor of the nasopharynx occurring almost exclusively in adolescent boys with the mean age of presentation at 15 years. The most common presenting symptom is nasal speech due to nasal obstruction or severe recurrent epistaxis. It is thought to arise near the sphenopalatine foramen at the junction between the nose and the nasopharynx at the root of the medial pterygoid plate. Extra nasopharyngeal spread is not uncommon at the time of presentation and this occurs to the retro antral region via the pterygopalatine fossa and anterior displacement of the posterior wall of antrum is

commonly seen. Further extension laterally to the infratemporal fossa occurs through the pterygomaxillary fissure subsequently it may spread to the orbit via the inferior orbital fissure, to the cavernous sinus and middle cranial fossa via the superior orbital fissure. Inferiorly it can bulge into the oropharynx and oral cavity. Two-thirds of cases show invasion of the sphenoid sinus implying an ICA supply whereas the lesion is typically supplied by the ipsilateral internal maxillary and ascending pharyngeal arteries.

Imaging features:

Juvenile angiofibroma appears on CT and MR images as a soft-tissue mass varying in size from a small nodule resting in the sphenopalatine foramen striding the choana to a large, locally aggressive growth extending in any or a combination of directions. Erosion of the pterygoid lamina on CT is probably a pathognomonic sign. On unenhanced CT scans the tumor appears isodense, on MR it displays intermediate signal on T1W and bright SIs on T2W images. The extent of the tumor and its characteristics are best evaluated by CE scans. Post contrast scans show intense enhancement with punctate areas of signal void indicating the highly vascular stroma. The following imaging-based grading system of juvenile angiofibroma has been proposed;

Grade I: Tumor confined to nasopharynx

Grade II: Tumor extending into pterygopalatine fossa or MS

Grade III: Tumor extending into orbit or intracranially.

The higher tumor vascularity contraindicates biopsy and preoperative embolization is necessary.

Benign Tumors of the Parotid

In the parotid gland, 70% are benign pleomorphic adenomas also termed benign mixed tumor. This tumor appears in later childhood or adolescence as a hard, mobile and painless cervical mass up to 7 cm in size. Most of the tumors are lateral to the plane of the facial nerve. It is a slow growing locally invasive lesion and complete surgical resection is important to avoid seeding of the adjacent tissues and recurrence. A small subset of these tumors (25%) contains Ca pleomorphic adenoma but if left untreated approximately 25% of pleomorphic adenomas undergo malignant change.

Imaging features:

Sonography shows a hypoechoic or relatively isoechoic lesion compared to the rest of the gland and may contain small calcifications. On CT and MR a well encapsulated, rounded, homogeneous soft-tissue density lesion with mild hyper intensity on T2W images is consistent with benign tumor

Warthin's Tumor

Warthin's tumor is also called adenolymphoma or papillary cyst adenoma lymphomatosum. This is the second most common benign parotid lesion comprising 2–10% of all parotid tumors. It presents as a multifocal, uni- or bilateral lesions in white population between 40 years and 70 years of age. Large tumors show cysts and nodules which distinguish them from lymph epithelial cysts.

Lipomas

Lipomas can arise within the parotid gland or may be a part of a lipomatosis syndrome. Lipomas are also common in the PPS

Imaging features:

CT scan shows a well-defined mass of fat density [−65 HU (Hounsfield units) to −125 HU]. On MR it follows the signal of subcutaneous fat on T1W and T2Wimages with loss of signal on fat suppression.

Neurogenic Tumors

Neurogenic tumors of the parotid can be either schwannomas or neurofibromas.

Imaging features:

Well-circumscribed ovoid lesions isodense to muscles on CT scan which show post contrast enhancement. There may be multiple lesions in neurofibromatosis type I while plexiform neurofibromas involve multiple compartments.

Hemangiomas and Lymphangiomas

Hemangiomas and lymphangiomas are uncommon salivary gland tumors. They have a striking female predilection and are most commonly seen in the parotid usually within him first 6 months of life, or later in childhood they have a spontaneous regression except when they have an arteriovenous fistula. Histologically they are capillary hemangioma, cavernous hemangioma, hemangioendothelioma and may have elements of lymphangioma.

Imaging features:

The gland may be involved diffusely or partially and may have a variable degree of abnormal vasculature depending on the size of the lesion. Color Doppler flow imaging (CDFI) shows the lesion vascularity. On CT and MR it appears as a cystic, vascular mass.

Malignant Tumors

Nasopharyngeal Carcinoma

Squamous cell carcinoma (SCCa) is the most common malignant tumor of the nasopharynx accounting for 70% of malignancies. Undifferentiated Ca and no keratinizing Ca are frequently associated with Epstein-Barr virus exposure and genetic susceptibility. There is a definite male preponderance with a mean age of occurrence in the 5th decade. Patients with early disease may be asymptomatic or have nonspecific symptoms. Most commonly overlooked signs are nasopharyngeal irritation or middle-ear effusion secondary to involvement of the Eustachian tube orifice. Most common presenting signs and symptoms are due to pharyngeal obstruction of the tumor, neck mass or nodal metastasis, tooth pain or loosening, proptosis and diplopia, trismus and headache implying involvement of the palate and alveolar ridge, orbit, infratemporal fossa or anterior skull base, respectively. The poster superior wall, lateral wall and anteroinferior walls are the common subsites of involvement.

Early cancer:

When the malignant lesion is small and localized the imaging appearance is similar to that of benign lesions. The earliest finding is blunting of the fossa of Rosen Müller. Airway asymmetry is not specific but muscle asymmetry is usually abnormal. Obliteration of the normally bright fat stripe of the parapharyngeal fat on T1W images may be one of the early findings. Obliteration of the pharyngeal orifice of Eustachian tube produces serous otitis media. There is an increase in the anterior superior width of adenoidal tissue which is normally less than 1 cm in adults. Involvement of the

ipsilateral deep cervical nodes of Rouvière is seen as low-to-intermediate signal on T1W and high signal on T2W.

The most reliable sign of nasopharyngeal malignancy is the detection of an aggressive mass infiltrating the deep fascial spaces around the nasopharynx. Nasopharyngeal CA's have a tendency to grow along the path of least resistance. Therefore, lateral spread to the PPS is most common and seen in 60% of patients. Further, it spreads to the MS and then spreads via a perineal infiltration of the mandibular nerve This acts as a "cable" along which the tumor tracks upwards to gain intracranial access through the foramen ovale to invade the Gasserian ganglion in Meckel's cave. Posterolateral spread to the retro styloid PPS with involvement of IX-XII cranial nerves, posterior involvement of the PVS and superior spread to the skull base and middle cranial fossa may occur in advanced disease. The aim of imaging is to define the tumor margins for the oncologist, provide accurate tumor staging and to evaluate the response to therapy. Identifying parapharyngeal infiltration is important as a parapharyngeal boost is given during radiotherapy to control lateral spread. Parapharyngeal spread precludes surgery or brachytherapy.

Imaging Features

There is no significant enhancement of the mass which is isodense to muscle on CT even when it is large. On plain MR the tumor is isointense to muscle on T1W and shows intermediate-to-high SI on T2W images. The T1W sequences valuable for detecting the replacement of high-signal fat in the deep fascial spaces with tumor. Fat-saturated post gadolinium T1W images are helpful in defining the extent of tumor infiltration into the marrow of the skull base.

Direct imaging signs of perineural spread are:

Thickening and enhancement of the affected nerves and abnormal enhancement in Meckel's cave and lateral bulging of the cavernous sinus dural membrane.

Indirect imaging signs include:

Foraminal enlargement on CT, Atrophy of muscles of mastication due to mandibular nerve infiltration, Obliteration of the normal fat plane in the pterygopalatine fossa in maxillary nerve infiltration. Post therapy evaluation to differentiate tumor mass from fibrous tissue can only be done by MRI. Mature scar is a form of dehydrated hypo cellular collagen which exhibits a dark signal on T2W with no contrast enhancement and can be distinguished from tumor tissue. However, an immature scar with hydrated hyper cellular granulation tissue cannot be differentiated from recurrent tumor based on MR signal characteristics because both show contrast enhancement and intermediate-to-high T2W signal. *Oropharyngeal Carcinoma*s in the nasopharynx SCCa constitute 90% of all malignant lesions of the oropharynx. Carcinoma arises most commonly from the palatine tonsils and base of tongue. Base of tongue Ca often arises on one side behind the circumvallate papillae and it is more aggressive and infiltrative than that involving the anterior two-thirds of the tongue due to the rich lymphatic network in this region. More than75% have internal jugular lymph node metastases at initial diagnosis and have an unfavorable prognosis. Differentiation between Ca and lingual tonsil at the tongue base is possible only on endoscopic biopsy.

Imaging features:

Invasion of deep fascial space, perineural infiltration, preepiglottic fat infiltration, bone invasion can be best visualized by cross-sectional imaging.

Non-Hodgkin's Lymphoma

Pharyngeal NHL arises from the rich extra nodal lymphoid tissue of the PMS, the tongue base or the palate. 60% of NHL occur in the head and neck and 60% arise in the extra nodal lymphoid tissue. It accounts for 20% of malignancies of the VS. Age of occurrence is in older men and majorities are of the histiocytic type.

Imaging Features

Imaging features are identical to those of the more common SCCa on both CT and MRI. Lymphomas tend to grow in circumferential manner without early invasion of the PPS but large lesions may invade the deep neck spaces, spread perineurally and invade the skull base in a similar pattern as SCCa.

Nasopharyngeal Rhabdomyosarcoma

Nasopharyngeal rhabdomyosarcoma is the most common soft-tissue sarcoma in children which can arise anywhere in the body. Within the head and neck the orbit and the nasopharynx are the most commonly involved areas. The age of incidence is below 15 years with a peak incidence of 2–5years and boys are more susceptible than girls. It accounts for 10% of malignant lesions arising from the VS. Rhabdomyosarcoma of the nasopharynx does not have any characteristic radiological appearance. The tumor appears as a bulky nasopharyngeal soft-tissue mass of intermediate SI on T1W-MR images with marked contrast enhancement. Subtle bony erosions are better demonstrated on CT scans while intratumoral hemorrhage and flow voids are well-depicted on MR

Malignant Tumors of the Salivary Glands

Mucoepidermoid Ca is the most common salivary malignancy in childhood. In adulthood they are more common than adenoid cystic in the parotid but the ratio is reversed in the submandibular gland. Adenoid cystic Ca is seen in the 5th and 6th decade and must be differentiated from Warthin's tumor for bilateral lesions. Tumors arising in the parotid gland from the deep lobe must be separated from a primary PPS salivary gland tumor. A primary PPS mass has a rim of parapharyngeal fat seen around the lesion. A mass may be predominantly in the PPS but if it has involvement of the superficial lobe of parotid it is likely to have originated from the deep parotid lobe. Salivary duct Ca is an uncommon aggressive malignancy primarily affecting the parotid gland. Metastasis from SCCa, elsewhere in the head and neck, melanoma of the scalp, basal cell Ca, gastrointestinal, lung, renal and breast cancer have been reported to metastasize to the parotid glands.

Imaging Patterns on CT and MR__

Lobulated pattern of encapsulation with mixed signal with cyst and necrosis represents an intermediate pathology. Poorly defined infiltrating mass with areas of high cellular density and necrosis or cyst formation indicates an aggressive pathology.

Primary Malignant Lesions in the Prevertebral Space

These are uncommon but invasion from an adjacent nasopharyngeal SCCa is not unusual. Metastasis to the vertebral body on posterior elements may be seen in lymphoma or leukemia. The most common primary malignancies that metastasize to the PVS include lung, breast, prostate, thyroid and renal cell Ca in adults. In children metastasis can occur from neuroblastoma, rhabdomyosarcoma and Ewing's sarcoma. The lesions may be lytic, sclerotic or mixed density typically presenting as expansile

lesions. Epidural spread at the time of diagnosis is frequently present. The spine is an area of vessel rich cellular marrow and MRI can detect metastasis not visible on plain films and before an osteoblastic reaction is detected on a bone scan. T1W-SE sequences display fat and water. Metastases have a signal lower than water and are easily seen in the yellow marrow. On T2W fat saturation and short-Tau inversion recovery (STIR) images, metastasis is relatively hyper intense to normal marrow indicating increased hyper cellularity. Osteoblastic/sclerotic metastasis remains hypo intense on all sequences. Other tumors of the PVS include chordomas and benign giant cell tumor, osteoblastomas, aneurysmal bone cyst and osteochondroma.

1.8 Masses of Neural Origin

Neurogenic tumors are the most common CS lesions.

There can also occur in the MS, the PPS and rarely the PS. Nerve sheath tumors of the neck may involve the vagus, hypoglossal, or cervical roots. Two types of tumors can arise from the nerves in the CS. Schwannomas are the most common tumors which originate from the Schwann cells surrounding the nerves. Most common is the tumor from the vagus nerve, less commonly the glossopharyngeal nerve, the ventral and dorsal cervical nerve roots, the cervical sympathetic chain and the brachial plexus. A tumor arising from the vagus nerve manifests as a mass in the anterior triangle, displacing the internal or common carotid artery anteromedial and the IJV posterolateral whereas a neoplasm of the cervical nerve roots manifest as a mass in the posterior triangle which may extend into one of the neural foramina of the cervical spine. Sympathetic chain tumors demonstrate a constant relationship with the longus colli muscles and lesions of the cervical sympathetic chain as they grow and expand, tend to push the common carotid, or internal and external carotids, anteriorly. Brachial plexus Schwannomas and neurofibromas in the IHN often displace the

anterior scalene muscle anteriorly. Schwannomas are well-encapsulated tumors that do not contain neural or collagen tissue but consists of cellular and myxoid components. The presence of these two components separate it from a neurofibroma.

Imaging Features

On CT the tumor is isodense with muscle and displays enhancement. The ICA is displaced anteriorly and laterally. In 20% of tumors hypodense areas reflecting cystic changes are visualized. Fluid-fluid levels may occasionally be observed in Schwannomas when they must be differentiated from lymphatic malformations. The fusiform shape on sagittal and coronal planes is well-demonstrated). On MR the tumor is hypo intense on T1W and hyper intense on T2W.Increasing cellularity of the lesion decreases the T2 relaxation time. Avascular Schwannomas can be well-differentiated from paragangliomas by the absence of flow void but vascular Schwannomas have identical imaging features to paragangliomas. This enhancement is due to extravasation of contrast from the abnormally permeable vessels and lack of draining veins. Dynamic scans can reveal the true nature of the lesion and differentiate it from hyper vascular lesions. The enhancement of the Schwannomas is seen at least 2 minutes after contrast injection and depicts the equilibrium phase of the contrast agent and the poor venous drainage of the tumor in contrast to paragangliomas which show a rapid filling and rapid wash out.

Neurofibromas

Neurofibromas are the second type of neurogenic tumors arising in the CS. In contrast to schwannomas, these are no capsulated and contain all elements of the nerve of origin and are continuous with it. The affected nerve is circumferentially compressed and diffusely penetrated by tumor elements and symptoms depend on the nerve

involved. Only 10% of patients of neurofibromas have neurofibromatosis and malignant transformation is more common in this group.

Imaging Features

The imaging features are dependent on the underlying histology with isodensity to muscle due to the collagen content. On CT neurofibromas show low attenuation due to lipid-rich Schwann and fat cells scattered in the tumor and there is no appreciable-contrast enhancement. The low density (near water) on CT is characteristic. Neurofibromas appear identical to avascular Schwannomas on MRI. They have a low SI on T1W and high SI on T2W images with variable enhancement.

Differentiation between neurofibromas and Schwannomas:

The imaging appearance of peripheral nerve sheath tumors depends on the histologic composition of the tumors and neurofibromas and schwannomas may be indistinguishable on imaging. However, there are some imaging findings that may be helpful in the distinction. Neurofibromas can be seen at any age. Schwannomas most commonly present between 20 years and 50 years of age with occasional occurrences in childhood. Neurofibromas are characteristically asymptomatic whereas schwannomas are often painful and tender. The pain may be localized or radicular in nature with associated paresthesias. Schwannomas have intermediateT1W signal and hyper intense T2W signal to muscle, with more uniform enhancement after contrast administration. Heterogeneous SI can be seen centrally in these tumors secondary-to-cystic degeneration and hemorrhage. Neurofibromas are hypo intense to isointense to muscle on T1W and hyper intense to muscle on T2W images. Variable enhancement is seen after contrast administration. Characteristic finding of neurofibromas is the

"target sign". On MRI an area of relatively hypo intense central signal with peripheral hyper intense signal is seen on T2W sequences which are characteristic.

1.9 Masses of Vascular Origin

Aneurysm

Aneurysm of the ICA is a vascular lesion of the neck. Helpful characteristics for differentiation of aneurysm from Schwannomas or other rare tumors are the peripheral calcification and the obliteration of the ICA lumen. CT and Angiography (MRA) can confirm the diagnosis of aneurysm.

Paragangliomas

Paragangliomas are slow-growing hyper vascular tumors arising from neural crest derivatives. They occur at multiple level within the CS including the carotid bifurcation (carotid body tumors), along the nodose ganglia of vagus nerve (glomus vagale tumors) and along the nerves supplying the jugular bulb (glomus jugular tumors).

Imaging Features

Glomus jugular tumor may cause variable erosion of the jugular foramen and typically produces a permeative pattern of destruction in contrast to a neurofibroma or Schwannoma which has a scalloped appearance. Glomus vagale and carotid body tumors often present as a pulsatile neck mass which may be multiple in 3–5% of cases. Paragangliomas are highly vascular tumors that enhance intensely on CT and MR They can be differentiated from Schwannomas and neurofibromas onia with the typical "salt and pepper" appearance. This is present due to multiple serpiginous vascular channels that produce the dark "pepper" and small hemorrhages that produce focal hyper intensities on T1 the "salt" appearance. Post contrast studies are helpful in

identifying small tumors and synchronous lesions. The nonchromaffin paragangliomas can occur as multifocal lesions, especially in patients with a family history of these tumors. Therefore, a study of both the right and the left carotid regions is necessary in these patients. Small tumors are ovoid or spherical while large tumors have a pear or dumb-bell shape with smooth contours.

Imaging features:

On MR these tumors have an intermediate SI on all sequences. Areas of necrosis or hemorrhages give rise to a nonhomogeneous appearance. Large tumors show serpentine channels of signal void due to tumor vessels with increased flow. Dynamic scanning reveals a sharp filling peak and a rapid washout of the tumor with a characteristic "dropout effect" on the dynamic MRI/CT. Angiography maybe done in patients with equivocal lesions and for therapeutic embolization. The differential diagnosis of these vascular lesions is metastasis from hypernephroma and papillary thyroid cancers. Other lesions, though rare, are metastasis from melanomas, extramedullary plasmacytomas, angiosarcomas and hemangiopericytomas.Some venous hemangiomas have similar imaging appearance with flow voids. A key feature for the differential diagnosis is the lack of displacement of adjacent vessels.

Diffusion-weighted Imaging in Paragangliomas

The addition of diffusion-weighted MRI and calculation of ADC values to routine MR protocols increases the accuracy of imaging in differentiating paragangliomas from other lesions that appear similar to paragangliomas on conventional MRI. It has been seen that depending on the tumor size the DWI and ADC show a high signal in paragangliomas. In comparison to the normal brain tissue of the cerebellum the calculated ADC is higher in paragangliomas. The high values of ADC in

paragangliomas compared to other lesions is because the mobility of water protons is relatively more free in the vascular architecture compared to the highly cellular dense skull base lesions, i.e., meningioma and giant cell tumor.

1.10 Masses of Mesenchymal Origin

Lipomatous tumors, such as lipoma, lipoblastoma and liposarcoma are the most common cervical neoplasms of mesenchymal origin. They typically manifest as painless masses, occurring most commonly in the midline of posterior neck or the posterior triangle. Cervical lipoblastoma typically presents as a rapidly enlarging mass. Liposarcoma is one of the most frequent malignant soft-tissue tumors in adults. It should be suspected whenever a large (5cm) fat-containing soft-tissue tumor is found, especially when it is clinically associated with pain and rapid growth. Well differentiated liposarcoma displays a hypodense fat density (<-20 HU) mass on CT; the tumor shows SIs similar to those of subcutaneous normal fat on MR images. Poorly differentiated liposarcoma displays tissue density on CT and low SI on SE-T1W and high SI on T2W-MR images with intense early enhancement on dynamic acquisition CE images Ill-defined borders and especially nonfat heterogeneous content indicate the high probability of malignant tumor. Other sarcomas that may be present are rhabdomyosarcoma, fibrosarcoma, osteosarcoma, chondrosarcoma, malignant fibrous histiocytoma leiomyosarcoma, alveolar soft part sarcoma and synovial sarcoma. The imaging findings of these entities frequently are nonspecific

1.11 Problem statement

Neck masses are associated with a diverse pathological spectrum with superficially located lesions(Rea, 2016; Stathakios & Carron, 2020). However, access is complicated by the structures of multiple small yet vital organ systems that are closely located in the neck hence presenting clinicians with a challenge in diagnosis of neck masses(Forghani, 2015). Histopathology of neck masses is a diagnostic gold standard while imaging (Ultrasound, CT, and MRI) has provided a non-invasive alternative for assessment of neck lesions(Brown & Harave, 2016; Pynnonen et al., 2017). Specifically, suprahyoid neck masses are difficult to assess by clinical inspection hence imaging is used to provide a precise evaluation (Kaur et al., 2017). In most cases, imaging by CT is done on SHN and the results confirmed by histopathological examination (Kaur et al. 2017). However, the cost of purchase, set up, human resource capacity, maintenance and geographical distribution of MRI and histopathological facilities have limited the availability of these diagnostic tools to clinicians especially in developing countries (Benediktsson et al., 2007; Haque et al., 2010; Kamel, 2011). Such factors have been associated with delayed or foregone diagnosis especially among patients from regions served by hospitals without histology labs coupled with their personal financial constraints that limit their ability to access these diagnostic tools from other hospitals(Adeyi & Olugbenga, 2011; Ali et al., 2018).

In Kenya, pathologies of the neck region account for a sizeable proportion of the admissions to the Ears, Nose and Throat (ENT) departments/facilities although their characterization and distribution is rarely evaluated(Muriithi, 2005). In addition, there is a disproportional distribution of CT scan machines within the country compared to histopathological laboratories. Specifically, the number of CT scans in Kenya has

increased by over 80% in the last decade while there is very limited capacity to perform histology at public laboratories(Brand et al., 2017; Korir et al., 2012). Data from other settings has shown evidence that CT imaging can provide accurate diagnosis of neck tumors and perform equally as well as histopathology (Shrestha et al., 2011).

However, despite the increased availability of CT imaging in Kenya, limited histopathology capacity has led to delayed diagnosis of neck cancers (Onyango & Macharia, 2006). A critical question would therefore be if CT imaging can be used to avert such delays as evidenced from other settings. So far, any form of data and/or literature from Kenya to support such evidence could not be easily retrieved by the researcher possibly implying that clinicians and radiologists in Kenya do not have local reference data to inform their practices.

1.12Justification

Reviewed literature has shown that neck masses have a significant contribution to the proportion of ENT cases in Kenya (Ayugi et al., 2011; Muriithi, 2005). In addition, significant strides have been made over the last decade on the development of diagnostic methods such as CT, MRI and histopathology (Brown & Harave, 2016; Forghani, 2015; Pynnonen et al., 2017). However, the cost implication limits the availability and usage of the histopathology and MRI across a wide geographical spectrum(Benediktsson et al., 2007; Haque et al., 2010; Kamel, 2011). On the contrary, CT imaging is widely available and provides essential information about the deep extension of clinically detected masses and may delineate additional clinically unsuspected lesions(Kadom & Lee, 2012).CT is better in showing the involvement of the bones and the extent of the lesions in soft tissues which MRI may not be able to(Haque et al., 2010).Good visualization using CT can be useful in providing

information to clinicians for improved patient management and next course of action planning as it assists clinicians diagnose and prognosticate patients with neck masses. Therefore, investigations on the possibility of using the more widely available CT imaging and comparison with histopathology results for assessment of SHN in Kenya can be used to avail and improve diagnosis hence informed patient care would be practiced especially in areas without histopathology laboratories.

1.13 Research questions

1. What are the types and anatomical location of masses identified in the suprahyoid neck masses using CT scan at MTRH?

2. What is the level of agreement between CT and histopathological suprahyoid neck masses diagnosis at MTRH radiology department?

1.14 Objectives

1.14.1 Broad objective

To determine the patterns of suprahyoid neck masses and their anatomical location using CT scan at MTRH radiology department.

1.14.2 Specific objectives

1. To evaluate the radiological characteristics of the suprahyoid neck masses identified using CT scan at MTRH radiology department.

2. To assess the anatomical location of neck masses involving the suprahyoid region at MTRH radiology department.

3. To determine the agreement between CT and histopathological suprahyoid neck masses diagnosis at MTRH radiology department.

1.15 Significance of the study

The findings of the study will be useful in understanding the common patterns and sources of suprahyoid neck masses and the agreement between CT and histopathology examination. This information will be useful to the hospital management for decision-making and planning purposes. It will also be useful to clinicians and radiologists in planning for the diagnosis and management of suprahyoid neck masses at the facility. The study will also be useful in providing relevant information to researchers and students with interest in this area which they can use for further studies on the subject.

CHAPTER TWO: LITERATURE REVIEW

2.1 Introduction

In this chapter, a review of literature on the suprahyoid neck masses as seen on CT and histopathology findings is presented.

2.2 Distribution of SHN masses seen at CT

A study of 117 patients, of which 59% were male, on the role of CT in the evaluation of neck masses established that common etiologies were infectious (17.9%) followed by ca larynx (14.5%) and swellings involving thyroid gland (11.1%)(Manohar B. Kachare & Amarnath R. Mohan, 2017). A study on neck masses among 50 patients in India reported that malignant masses accounted for 84.2% and 9.6% of the observed 19 nodal and 31 non nodal masses respectively(Ajay K Goutam et al., 2017). A separate study of 60 patients, in the same country on assessment of SHN masses via CT, established that squamous cell carcinoma was the predominant etiology at 30% of all SHN masses observed and those localized in the prestyloid parapharyngeal space which had the highest number of lesions (Kaur et al., 2017).

In Mangalore, 53% of 100 patients had malignancies which were predominantly squamous cell carcinoma at 43% of all observed cancers. In addition, 20% of the lesions were of an infective origin while 23 % were benign and congenital cystic lesions(Shrestha et al., 2011). At the Kenyatta national hospital (KNH) in Kenya, an assessment by CT and histopathology of 42 patients reported carcinoma of the larynx/hypopharynx and nasopharyngeal tumors constituted 57% cases seen. In addition, inflammatory lesions included submandibular abscess, inflammatory pharyngeal polyps, pharyngeal mucosal adenoids and cervical lymphadenopathy(Muriithi, 2005).

An evaluation of palpable neck masses comparing ultrasonography and CT on 40 patients aged 3 to 80 years identified lesions to be inflammatory (17.5%), Developmental (7.5%), Thyroid masses (30%), Mesenchymal (10%), Neural (5%), Vascular (5%), Bone (5%), Lymph nodes (10%) and Salivary gland mass (10%)(Pratap et al., 2013).

2.3 Effectiveness and accuracy of CT in neck masses diagnosis

Several studies have made an assessment of the diagnostic performance of CT imaging in relation to other diagnostic methods such as histopathology and ultrasonography. In India, CT had a higher diagnostic accuracy of 94% compare 76% of ultrasonography while both yielded an accuracy of 94% (Ajay K Goutam et al., 2017). A separate study established that CT had an excellent correlation with histopathological findings with sensitivity of 96.4%, specificity of 100%, positive predictive value of 100% and a negative predictive value of 91.67%(Kaur et al., 2017). In Malangore, the diagnostic accuracy of CT in the evaluation neck masses gave a sensitivity of 96.5% and specificity of 100% in a study while the positive and negative predictive values were 100% and 95.2% respectively (Shrestha et al., 2011).

Multislice spiral CT was used to evaluate neck masses among 45 patients and established 97% and 100% accuracy rates of predicting the nature (benign or malignant) and the exact extent of the mass respectively. However, the accuracy for predicting the final histopathological diagnosis was 62%. In addition, the extent of the pathology, the local or contiguous spread, and vascular involvement, predicted by multislice CT examination, corroborated well with the surgical findings for all cases observed (Gupta P et al., 2013).

CT was established to have an accuracy of 76% in predicting the final pathological diagnosis of neck masses compared to MDCT which had predicted the benign or malignant nature of the mass and its extent were reported at 98% and 100% respectively. In all 100 cases in the study, the pathology's extent, the local or contiguous spread, and vascular involvement predicted by MDCT examination corroborated well with the surgical findings(Ravi N et al., 2015). At KNH, that CT imaging had a sensitivity of 83.3% (Muriithi, 2005)

2.4 Histopathology of neck masses

Histological patterns and/or sub-patterns are characteristic of particular tumors or groups of tumors; hence, these particular patterns are essential for the histopathological diagnosis. The knowledge of various patterns and sub-patterns in different tumors helps diagnose and deliver appropriate treatment. The basis for different tumor patterns is thought to be the epithelial-mesenchymal cell interaction as well as the interaction of various cytoskeletal organelles of these cells. Epithelial-mesenchymal transition (EMT) has been postulated as a versatile mechanism that facilitates cellular repositioning and redeployment during embryonic development, tissue reconstruction after injury, carcinogenesis, and tumor metastasis(Tarin, 2012)

The main histological patterns encountered in head and neck tumors include glandular/pseudo glandular, non-glandular epithelial/epithelioid pattern, round cell pattern, spindle cell pattern, biphasic pattern, and surface epithelial patterns associated with or affected by the neoplastic process(Dive et al., 2014).

These main patterns are further subdivided into different sub-patterns as shown in the table below;

Table 1.1: Main Histopathology patterns

Serial number	Histological patterns	Lesions/conditions where encountered
A	Glandular/pseudoglandular	
A1	Tubular pattern	Adenoid cystic carcinoma and Basal cell adenoma
A2	Acinar/microacinar pattern	Acinic cell carcinoma of salivary gland
A3	Cribriform pattern	Adenoid cystic carcinoma
A4	Follicular pattern	Acinic cell carcinoma, clear cell carcinoma, follicular ameloblastoma
A5	Microcystic/mucinous pattern	Acinic cell carcinoma
A6	Canalicular pattern	Salivary gland adenoma or carcinoma
A7	Hobnail pattern	Hemangioendotheliomas, angiosarcoma
A8	Slit-like pattern	Angiosarcoma
A9	Pseudoglandular pattern	Adenoid basal cell carcinoma, squamous cell carcinoma, myxoid liposarcomas
B	Nonglandular/epithelial/epithelioid pattern	
B1	Basaloid pattern	Basal cell carcinoma, cylindroma, basal cell adenoma, basal cell hyperplasia, basal cell ameloblastoma
B2	Comedo pattern	Salivary duct carcinoma/terminal duct carcinoma
B3	Alveolar pattern	Rhabdomyosarcoma, malignant melanoma, intradermal naevi (traumatized)
B4	Packeted pattern	Malignant melanoma
B5	Palisading pattern	Basal cell carcinoma, schwannoma, palisaded encapsulated neuroma, keratocystic odontogenic tumor (basal layer)
B6	Reticular/lattice pattern	Acinic cell tumor
B7	Squamoid pattern	Adenocarcinoma, malignant melanoma, Spitz nevus
B8	Trabecular pattern	Merkel cell tumors, smooth muscle tumors and Basal cell adenoma
B9	Desmoplastic/scirrhous pattern	Basal cell carcinoma, sclerosing fibrosarcoma
B10	Pseudocystic pattern	Myxoid liposarcoma
C	Round cell pattern	
C1	Diffuse pattern	Lymphoma, leukemia, small cell undifferentiated carcinoma, Ewing's sarcoma, Merkel cell tumor, malignant melanoma
C2	Septate/lobulated pattern	Ewing's sarcoma, alveolar rhabdomyosarcoma
C3	Alveolar/pseudoalveolar pattern	Alveolar rhabdomyosarcoma
C4	Round cell pattern with rosettes	Adenomatoid odontogenic tumor, Primitive neuroectodermal tumor, neuroblastoma
D	Spindle cell pattern	
D1	Diffuse monomorphic bland pattern	Fibromatosis, benign neurofibroma, schwannoma, smooth muscle tumors
D2	Diffuse monomorphic highly cellular pattern	Malignant peripheral nerve sheath tumor, malignant melanoma
D3	Pleomorphic spindle cell pattern	Malignant fibrous histiocytoma
D4	Spindle cell pattern with prominent sclerosis	Sclerosing liposarcoma, desmoplastic melanoma, epithelioid sarcoma, sclerosing fibrosarcoma
D5	Whorled/storiform pattern	Benign and malignant fibrous histiocytoma
D6	Hemangiopericytomatous pattern	Hemangiopericytoma, solitary fibrous tumor, mesenchymal chondrosarcoma
E	Biphasic pattern	Malignant peripheral nerve sheath tumor, malignant melanoma
F	Surface epithelial patterns	
F1	Lichenoid reaction pattern	Seborrheic and solar keratosis, flat wart, intraepidermal carcinoma, lichen planus-like keratosis, lichenoid reaction
F2	Psoriasiform pattern	Mycosis fungiodes, clear cell acanthoma
F3	Clear cells within epidermis	Verrucous carcinoma, clear cell variant of squamous cell carcinoma, clear cell acanthoma
F4	Dysplastic changes of epithelium	Hyperkeratosis complex, actinic keratosis, carcinoma *in situ*
F5	Pseudoepitheliomatous hyperplastic pattern	Malignant melanoma, Spitz nevus, granular cell tumor
F6	Pattern with cup-shaped/inverted lobules of squamous epithelium	Follicular keratosis, keratoacanthoma, warty dyskeratoma, molluscum contagiosum
F7	Nesting/clonal proliferation (Borst-Jadassohn pattern)	Clonal seborrheic keratosis, intraepidermal basal cell carcinoma, intraepidermal squamous cell carcinoma, malignant melanoma
F8	Pagetoid pattern	Superficial spreading malignant melanoma
F9	Elongated anastomosing strands	Fibroepithelial variant of basal cell carcinoma, reticulated seborrheic keratosis
F10	Verrucous pattern	Seborrheic keratosis, condyloma acuminatum, viral wart, verrucous carcinoma, verrucous xanthoma

Courtesy: Modified from the reference given below: Awatif I Al-Nafussi. Common histological patterns and cell types of tumors. In: Awatif I Al-Nafussi. Tumor diagnosis: Practical approach and pattern analysis, 2nd edition. London: Hodder Arnold; 2005. p. 3–62

Adopted from: Dive et al., (2014)

2.5 Imaging of the neck using MDCT

Multi-slice CT (MDCT) is quickly becoming the new standard in radiological imaging. Between 1998 and 2000, during the introduction of MDCT into the routine clinical diagnosis, the advantages in cardiovascular-, thoracic- and abdominal-imaging were evident, while the position of MDCT use in head/neck imaging was relatively unclear. The head and neck region presents difficult anatomy and physiology for imaging. Almost no other anatomical region in the human body needs such a high level of resolution and additional functional information. There exist the most dense and most thin bones in the human body and very delicate soft tissues. All these factors are enormous technical challenges for any CT machine(Reiser et al., 2012).

MDCT has higher resolution, shorter examination time and the acquired data can be subjected to volume rendering and a tailored contrast application (Imhof et al., 2003).The reduced examination time significantly lowers the risk of motion artifacts, for example, those caused by breathing, swallowing, and patient motion(Gupta P et al., 2013; Imhof et al., 2003; Ravi N et al., 2015). However, gains in examination time may be lost in post processing and reporting. The radiation dose must be kept low, using what is necessary rather than possible, and mages should be generated with the maximum acceptable noise level (Imhof et al., 2003).

It is also possible to carry out Valsalva- or phonation-studies to visualize the glottis and vocal cords. MDCT allows high-resolution imaging with 0.5 mm slice thickness and multiplanar reconstructions (MPRs) in all planes (nearly isotropic) without loss of detail resolution (Philips DX 8000 maximal variation in the z-axis: S0.69/0.99 mm). The length of time of contrast medium administration must be reduced, which lowers

the volume required and necessitates high-concentration medium use(Whyte et al., 2017).

Usually, any abnormality in medical imaging should be visualized in at least two planes; the head and neck axial and coronal planes are the most common ones. With earlier CT Scanners, two examinations with doubled radiation exposure were necessary. With MDCT, these planes can be obtained in a single examination by isotropic reconstruction, saving both time and radiation exposure to the patient. Retakes due to motion artifacts are much rarer than with previous scanners(Reiser et al., 2012). Overlapping scans, which increase scanning time and radiation, are replaced by the possibility of calculating arbitrarily many overlapping images from one MDCT scan without renewed exposure. Standard protocols have been recommended. KVp is changed on a regular basis and contrast medium is used routinely except for visualizing the temporal bone or the osseous structures of the paranasal sinuses. In the larynx, biphasic application of contrast injection is used, particularly when viewing carcinoma(Seeram, 2013).In head and neck radiology MDCT is touted to become a no avoidable standard within the next years(Imhof et al., 2003).

2.6 Contrast medium

Several comparative studies have reported that the peak of the density/time curve is higher and reached earlier and the curve slope is steeper for high concentration contrast material(Iomeron (R) 400 (400 mg of iodine/ml)) compared to lower concentration contrast medium ranging between 300 mg/ml to 350 mg/ml (Guerrisi et al., 2011; Jo et al., 2016; Romano et al., 2009). These are essential factors to consider since good contrast enhancement is essential for visualizing structures such as normal soft tissue structures or carcinoma(Imhof et al., 2003).

Differentiation between normal and abnormal soft tissue, rather than between the surrounding vessels and the tumour, is a major problem. The degree of contrast obtained is low because hypovascular tumours do not rapidly take up much contrast material(Seeram, 2013). In addition, the peak contrast density are known to differ from one tumour to another hence the contrast protocol needs to be tailored to the patient and fusion of timely different images is advisable (Baum et al., 2000).

The effect of contrast medium concentration was also studied in 35 patients with malignant facial tumors of which 18 were administered standard contrast medium and 17 received high-concentration contrast medium. Results on the absolute tumor density was less than expected. (109 for the Iomeron 300 group and 112 for the Iomeron 400 group) with a high degree of density variation (Imhof et al., 2003).

.However, there was a high degree of density variation, which was at least 5-10% in the tumour. It is important to examine a large number of individuals in a study such as this to obtain meaningful results (Imhof, 2003).

Findings that high concentration contrast medium produces a greater degree of contrast enhancement is more time-critical and fits better to the lower scan times of the most recent 16- row MDCT scanners compared to standard concentration contrast medium can be used to develop patient care protocols (Imhof et al., 2003).

CHAPTER THREE: METHODOLOGY

3.1 Study setting

The study was carried out at the Radiology department of the Moi Teaching and Referral Hospital (MTRH). MTRH, located in Eldoret town within Uasin Gishu County, is the second largest public referral facility in Kenya after Kenyatta National Hospital. It has a large catchment area that includes all counties in Western Kenya and most former Rift Valley province. It also receives patients from neighboring countries, including Uganda, Rwanda, Tanzania, and South Sudan. It has a bed capacity of 800 beds(Benjamin Odhiambo Bonyodon, 2015; Mohamed et al., 2020; Sitienei et al., 2018).

The radiology department has fourteen radiologists, of which four are from Moi University's department of radiology. The department has two CT scan machines and one MRI machine. Daily, approximately fifty CT scans and ten MRI scans are carried out.

3.2 Study design

A cross-sectional study design.

3.3 Study population

Patients referred to the radiology department with neck masses and diagnosed with Suprahyoid Neck massed on CT formed the study population.

3.4 Sample size

The radiology department serves between 100 and 140 patients with SHN in a year based on a review of registry records from the year 2010 to 2015. Therefore, in this study no sampling was conducted due to the small number of patients presenting to the department with SHN.

3.5 Sampling technique

A census of all patients with SHN masses presenting to the radiology department in the period January to December of 2016. This census approach was adopted due to the small population size observed each year at the department hence achieve a desirable level of precision.

3.6 Eligibility criteria

3.6.1 Inclusion criteria

Patients presenting with suprahyoid neck masses as diagnosed by CT scan who consented to participate in the study.

3.6.2 Exclusion criteria

All patients who had received any form of therapeutic intervention for SHN, including surgery, chemotherapy, and radiotherapy, were excluded.

3.7 Data collection

CT was done, and the site, size, and extent of the lesion were evaluated. The margins, relation to adjacent structures, and the tissue attenuation values were also evaluated. Attention was paid to the cranial and caudal extension of the lesion, contrast enhancement, effect on adjacent tissues.

The CT images were then evaluated for size, location, contour, calcification, type of enhancement, necrosis, and fat planes with the adjoining structures, lymph nodes, and other supplementary CT findings including shape, infiltration and mass effect.

The following radiological descriptions were used in the categorization of suprahyoid masses. Malignant lesions were those that demonstrated contrast enhancement, invasion of adjoining soft tissues, invasion of the bones, and likely perineural spread.

Inflammatory lesions were those which demonstrate absent or peripheral enhancement in post-contrast images and those associated with the presence of other inflammatory changes in the adjacent structures. Based on the patient's age, symptoms, clinical and CECT findings, a provisional diagnosis was made. For those patients who will require confirmatory histopathological examination, the test will be ordered, and the results compared to the provisional CT diagnosis made.

Images were acquired as follows. (Summary)

Patients lied supine with hyperextended neck. Scanogram was in the lateral view. Axial slices covered the area from the hyoid bone to the skull base. Scan intervals were between 3-5mm sections. Slices was parallel to lower edge of mandible. Images was acquired during quiet respiration, no swallowing. An intravenous, non-ionic water-soluble contrast agent (iohexol) 75 -100 ml were used in quantities varying with the body weight. Soft tissue windows for all images, with additional bone windows to evaluate for bone or cartilage invasion. CT scan used was the Siemens Somatom 32 slice scanner.

Preparation

Nil per oral 4 hours before contrast administration.

Clinical data, laboratory findings reviewed before imaging.

Patients to change to hospital gowns to avoid artifacts like zips, buttons, jewelry, etc.

Procedure was explained to patient and informed consent obtained.

Positioning

Supine

Headfirst

Posterior neck support to align neck plane.

Instructions

Usually quiet breathing without swallowing

On special cases, may be instructed to hum, puff mouth or hold breath.

Planning and scanogram

To use neck pre/post IV contrast.

Topogram length 256mm, from skull base to aortic arch level.

Pre contrast scanning, length as topogram, scanning done caudocranial or craniocaudal.

Acquisition; 5mm

Reconstruction; provision of at least up to 1.5mm

Technical factors; KV 130/110/80 depending on patient's size. MAs; 80

Post contrast scanning; length as topogram or as necessary.

Acquisition; 5mm or 3mm

Reconstruction; provision for at least up to 1.5mm

Contrast injection; bolus tracking or hand injection

Duration; approximately 3 min

Viewing to be done on PACS console in radiology reporting rooms. View in axials, coronals, and sagittal views.

Slice thickness for printing set at 1.5mm

3.8 Data analysis

The collected data was entered into MS Excel and thereafter data cleaning and coding was performed. Measures of central tendency (mean, median, and mode) were used to give summaries of continuous variables such as age. Categorical variables were summarized using counts and proportions. The McNemar's test was used to compare the marginal proportions of SHN malignancies identified by CT and histopathology. In this test, the null and alternative hypotheses are stated as:

$$H_0: p_{CT} = p_{Hist}$$
$$H_1: p_{CT} \neq p_{Hist}$$

Where p_{CT} and p_{Hist} represent the proportion of suprahyoid neck masses identified by CT scan and histopathology respectively. Using histopathology as the gold standard test, sensitivity and specificity of CT imaging on identifying the nature of the tumor (malignant or benign) were conducted. All data analysis was conducted using the Statistical Package for Social Sciences (SPSS) version 23.0.

3.9 Data presentation

The output was presented in form of summary tables, graphs, radiological images, and prose form.

3.10 Ethical considerations

Permission to carry out the study at MTRH was sought from the hospital management. Ethical review and approval was given by Moi University/ MTRH Institutional Research Ethics Committee (IREC)

The nature and purpose of the study was explained to the study participants using a language the participants were comfortable with and information leaflets given to them. The consent form was translated to Kiswahili. Written consent was sought from the respondents. For children below the age of 18 years, and above 7 years, assent was sought from them while consent was sought from their parents or guardians. Participation was voluntary and no one was coerced to participate.

The information collected from the respondents was kept securely in lockable lockers and entered in a password protected laptops. The information was anonymized using pseudo names and was only shared between the student and the supervisors.

3.11 Study pre-test

A pre-test study was carried out among the 10 patients with suprahyoid neck masses. The results of the pilot study showed that the study tools were reliable and valid. Reliability was established by using the data collection tool in the pilot study and the radiology assistant asked to leave out any sections that were found ambiguous or were not clear. In this study validity was taken to mean the extent to which the data collection instruments covered the objectives. To determine content validity of the instruments, supervisors, colleagues and several subject experts from the Department of radiology and the college of health sciences were consulted. Advice given by these individuals helped the researcher determine the validly of the research instruments. This was then used in making necessary changes.

CHAPTER FOUR: RESULTS

4.1 Introduction

In this chapter, the results of the study are presented. The chapter is divided into four sections. The first part presents demographic information of the patients.

4.2 Demographic information

A total of 123 patients were recruited into the study of which 80 (65.0%) were males while 43 (35.0%) were females (Figure 4.1).
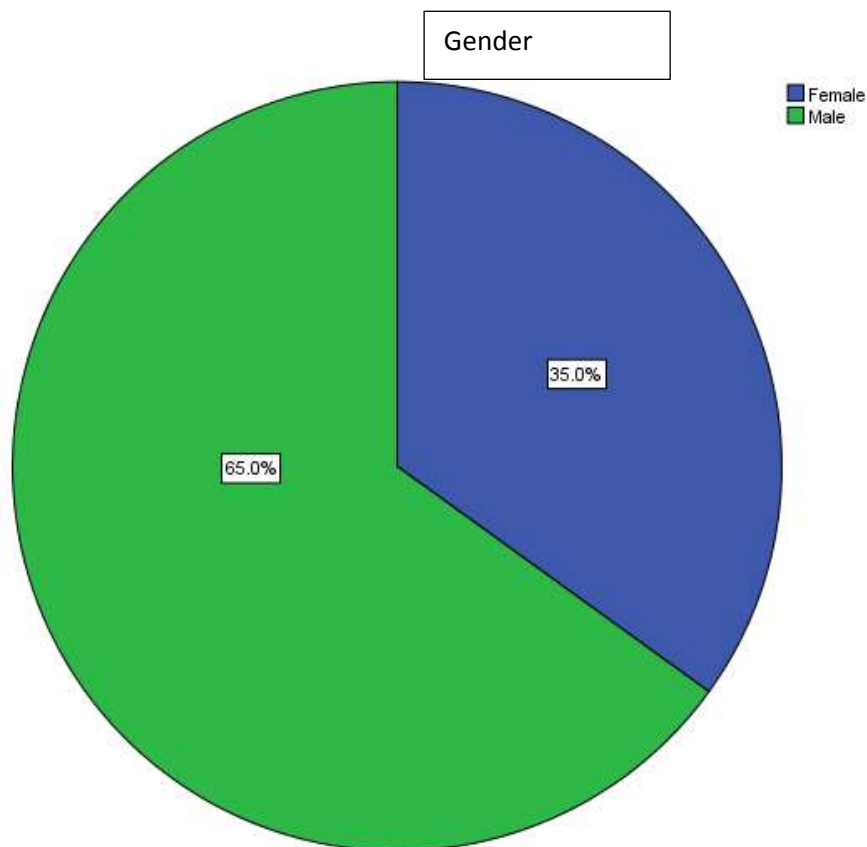
Figure 4.1: Gender of participants

The mean age of the patients was 44.6 ±16.6 (SD) years. The youngest participant was 1 year and oldest was 86 years (Figure 4.2) while majority of the participants (86.9%) were aged between 18 and 69 years.
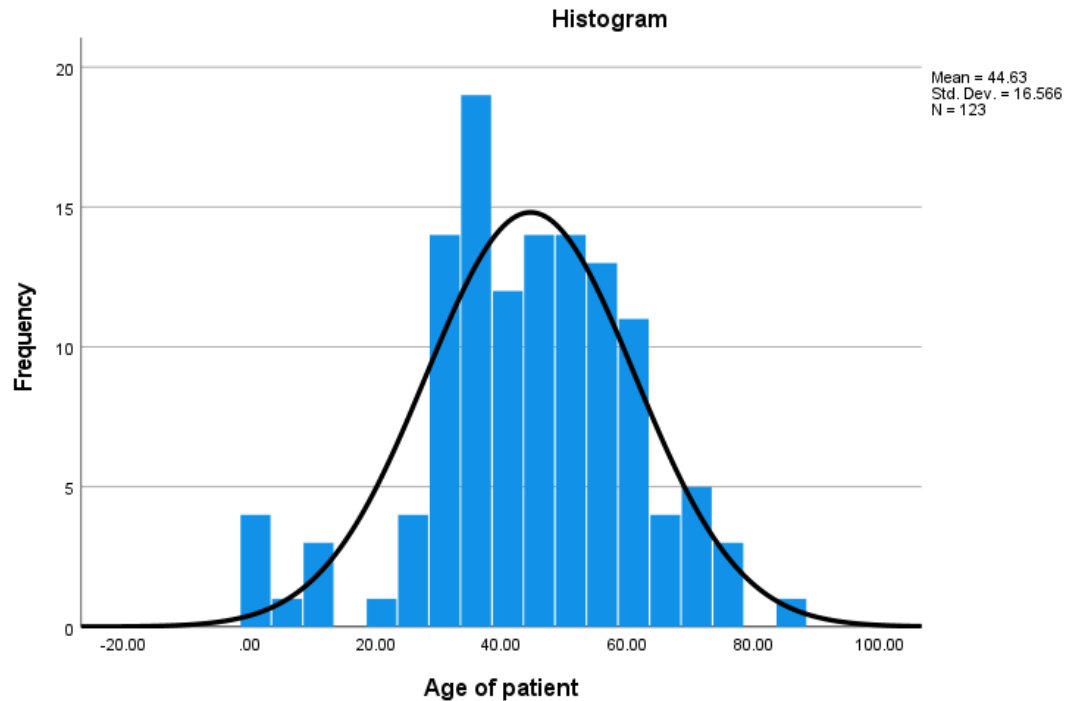
Figure 4.2: Age distribution of participants

The age distribution by age bands is presented in table 4.1 below. Out of the 123 study participants, 49 (39.8%) were aged 36-52 years, 32 (26.0%) were 53-69 years, 26 (21.1%) were 18-35 years, 8 (6.5%) 70 years and above and 8 (6.5%) 1-17 years.

Table 4. 1: Age distribution of study participants

Age group	Frequency (n)	Percent (%)
1- 17 years	8	6.5
18- 35 years	26	21.1
36-52 years	49	39.8
53- 69 years	32	26.0
70 years and above	8	6.5

4.3 Anatomical location and patterns of suprahyoid neck masses

Of the 123 cases of suprahyoid neck masses, 38 (30.9%) were found in the Pharyngeal Mucosal space, 26 (21.1%) parotid space, 13 (10.6%) retropharyngeal space, 13 (10.6%) post styloid parapharyngeal space, 12 (9.8%) Masticator space, 7 (5.7%) Pre-styloid parapharyngeal space, 7 (5.7%) prevertebral space, and one (0.8%) sublingual space (Figure 4.3).
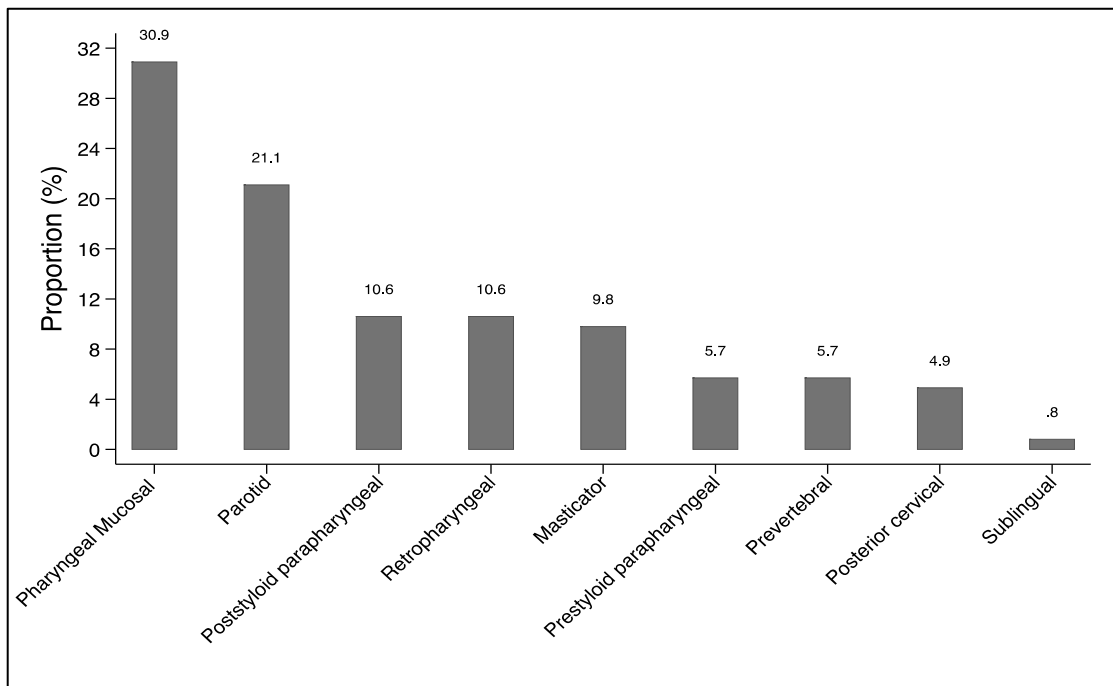
Figure 4.3: Anatomical spaces with masses

The etiology (Figure 4.4) of the identified SHN masses, in descending order, was: malignant 55 (44.7%), benign 27 (22.0%), infectious 25 (20.3%), inflammatory 7 (5.7%), congenital 6 (4.9%) and traumatic3 (2.4%).
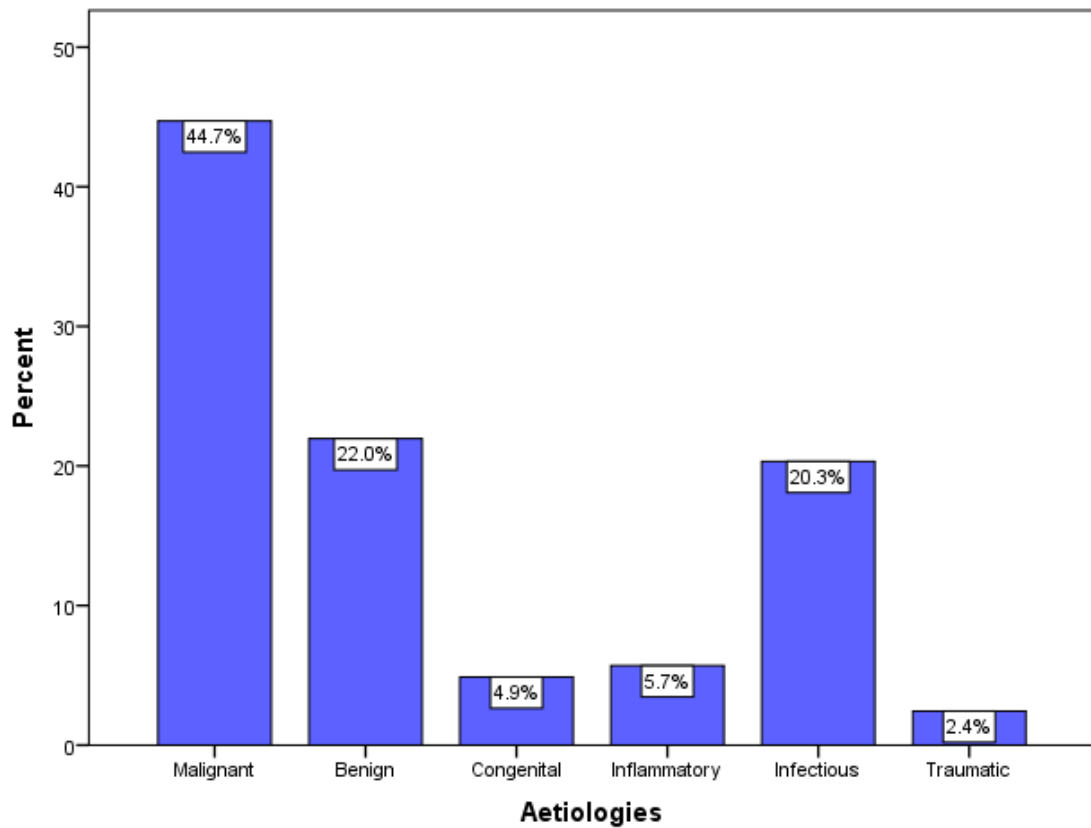
Figure 4. 4: Types of SHN masses identified at MTRH radiology department

Of the 55 malignant masses, 24 (43.6%) were in the Pharyngeal Mucosal space, 12 (21.8) in the parotid space, 6 (10.9%) in the masticator space, 6 (10.9%) in the Prestyloid parapharyngeal space, 5(9.1%) in the retropharyngeal space, 1 (1.8%) in the sublingual space and 1 (1.8%) in the Post styloid parapharyngeal space (Figure 4.2).

Table 4. 2: Etiologies with respect to spaces

Space	Aetiologies						Total
	Malignant	Benign	Congenital	Inflammatory	Infectious	Traumatic	
Masticator space	6	2	1	0	3	0	12
Parotid space	12	9	3	2	0	0	26
Pharyngeal Mucosal space	24	5	0	2	7	0	38
posterior cervical space	0	2	2	0	1	1	6
Carotid/ Post styloid parapharyngeal space	1	8	0	0	4	0	13
Prestyloid parapharyngeal space	6	1	0	0	0	0	7
Prevertebral space	0	0	0	0	5	2	7
Retropharyngeal space	5	0	0	3	5	0	13
Sublingual space	1	0	0	0	0	0	1
Total	55	27	6	7	25	3	123

Out of the 123 SHN masses observed at the radiology department, 60 (48.8%) had heterogeneous enhancement, 28 (22.8%) had rim enhancement, 22 (13.0%) had homogenous enhancement and 13 (10.6%) had no enhancement (Figure 4.5).
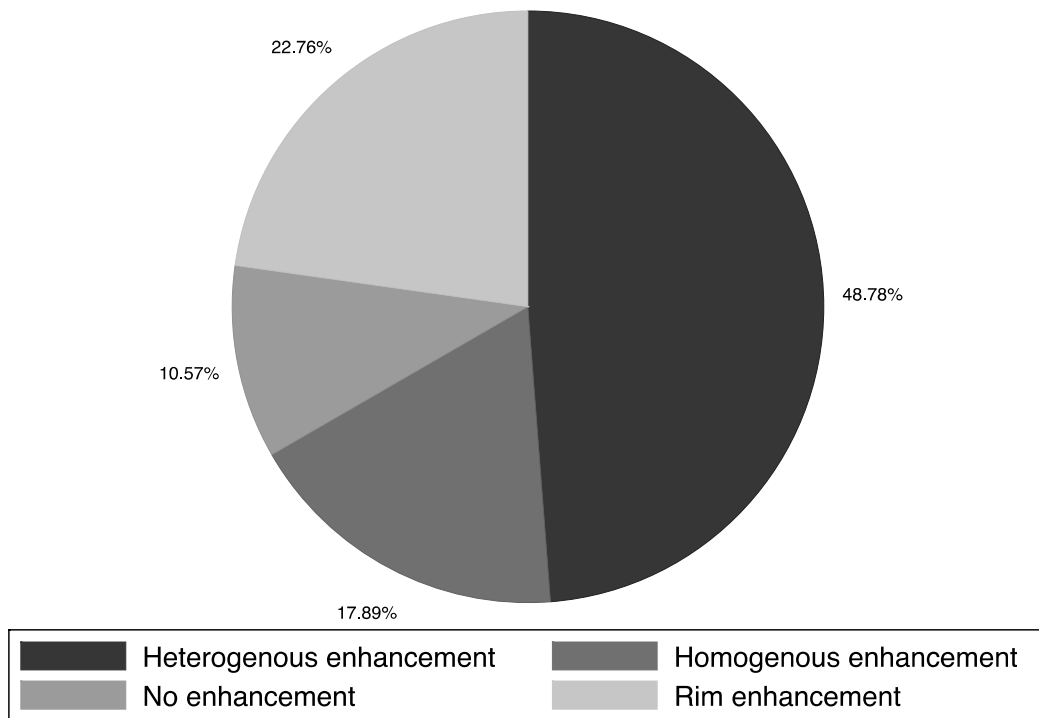
Figure 4. 5: Pattern of enhancement of SHN masses assessment by CT imaging

The frequency distribution of SHN mass diagnoses identified by CT scanning table 4.3 showed that the leading diagnoses were abscesses 21(17.1%), metastases 17 (13.8%), parotid tumor 15 (12.2%), oropharyngeal cancer 11(8.9%), Osteomyelitis 5 (4.1%) and sarcoma 5 (4.1%).

Table 4.3: CT diagnosis of SHN masses at MTRH

CT Diagnosis	Frequency (n)	Percent (%)
Abscess	21	17.1
Metastases	17	13.8
Parotid tumour	15	12.2
Oropharyngeal Cancer	11	8.9
Osteomyelitis	5	4.1
Sarcoma	5	4.1
Paraganglioma	4	3.3
Schwannoma	4	3.3
Squamous cell ca	4	3.3
Tonsillitis	4	3.3
Lipoma	3	2.4
Lymphangioma	3	2.4
Ca base of tongue	2	1.6
Carotid space cellulitis	2	1.6
Cystic hygroma	2	1.6
Lymphoma	2	1.6
Brachial cleft cyst	1	.8
Dermoid cyst	1	.8
Fragmented vertebral fracture	1	.8
Hematoma	1	.8
Internal carotid aneurysm	1	.8
Leiomyoma	1	.8
Lymphadenitis	1	.8
Lymphadenopathy	1	.8
Mandibular Osteosarcoma	1	.8
Minor salivary gland tumour	1	.8
Osteosarcoma	1	.8
Parotid adenoma	1	.8
Parotid adenopathy	1	.8
Parotitis	1	.8
Reactive adenopathy	1	.8
Sialolithiasis	1	.8
Stensen duct stone	1	.8
Tonsillar cancer	1	.8
Vertebral fracture with soft tissue swelling	1	.8

A scan showing identification of abscess in the retropharyngeal and parotid spaces is

shown in Figure 4.6 and in figure 4.7 a contrast of carotid space showing

identification of paraganglioma is presented. The first image shows hypoattenuating lesions in the retropharyngeal and posterior cervical spaces. There is peripheral enhancement. The retropharyngeal mass displaces the parapharyngeal fat anteriorly. The second image show and avidly enhancing right carotid enhancing mass with displacement of the parapharyngeal fat anteromedially.

A total of 108 (87.8%) histopathological diagnoses were successfully made while 15 were not biopsied. Diagnoses at the pharyngeal mucosal space accounted for 35.2% of the total histopathological diagnoses made of which 11 (28.9%) were identified as cancer of the pharyngeal. In addition, 26 (22.0%) diagnoses were made from samples extracted from the parotid space of which 14 (53.4%) showed parotid cancer. In table 4.4, a summary of the total number of diagnoses, common diagnoses and their respective numbers is provided.
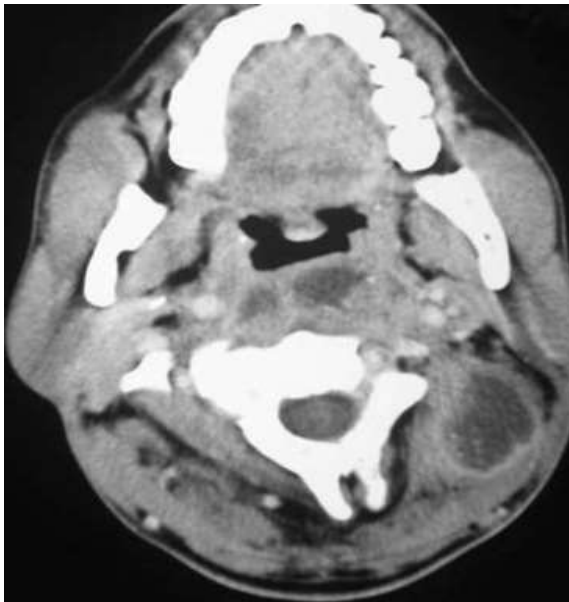
Figure 4.6: Abscesses in the retropharyngeal and parotid space on CT
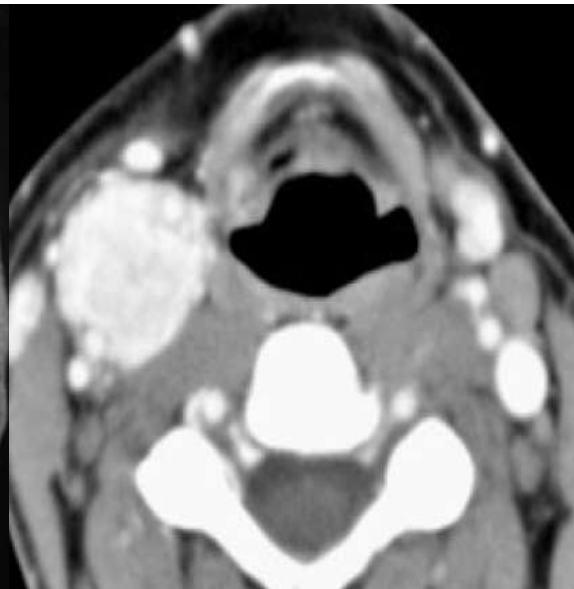
Figure 4.7: Paraganglioma on contrasted CT in Carotid space

Table 4. 4: Spaces and common pathology

Space	Total number of diagnoses	Common diagnosis	No of common diagnosis (%)
Retropharyngeal space	13	Abscess	7 (53.8%)
Prevertebral space	7	Osteomyelitis	5 (71.4%)
Parotid space	26	Parotid tumor	14 (53.8%)
Postsyloid parapharyngeal space	12	Paraganglioma	4 (33.3%)
		Schwannoma	4 (33.3%)
Prestyloid parapharyngeal space	7	Metastases	6 (85.7%)
Masticator space	12	Sarcoma	5 (41.2%)
Pharyngeal mucosal space	38	pharyngeal ca	11 (28.9%)
Posterior cervical space	6	Cystic hygroma	2 (33.3%)
Sublingual space	1	Ca base of tongue	1 (100%)
Carotid space	1	Abscess	1 (100%)

There was presence of necrosis in 82 (66.7%) of the cases (Figure 4.8). Out of the 55 malignancies, necrosis was identified in 39 (70.9%) participants of which majority (n=18; 46.2%) were in the pharyngeal mucosal space, followed by 8 (20.5%) in the parotid space, 5 (12.8%) in the prestyloid parapharyngeal space and 4 (10.3%) in each of masticator and retropharyngeal spaces.
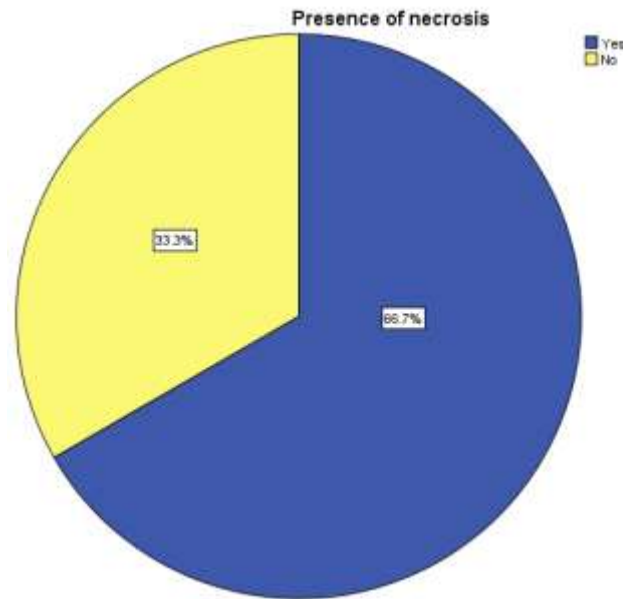
Figure 4.8: Presence of necrosis among all study participants.

The main features of the SHN masses observed on CT were necrosis, enhancement, and margins. Of the 123 cases, necrosis was observed in 82 (66.7%) cases, well-defined margins in 69 (56.1%) cases and enhancement in 110 (89.4%). The distribution of these features in relation to the spaces is shown in table 4.5 below.

Table 4. 5: CT features of the different pathologies in the different spaces

Anatomical space	Necrosis	well-defined margins	Enhancement
	n (%)	n (%)	n (%)
Masticator space	9 (11.1%)	5 (7.2%)	12 (10.9%)
Parotid space	13 (15.9%)	11 (15.9%)	23 (20.9%)
Pharyngeal Mucosal space	32 (39.0%)	17 (24.6%)	37 (33.6%)
posterior cervical space	1 (1.2%)	6 (8.7%)	2 (1.8%)
Post styloid parapharyngeal space	6 (7.3%)	12 (17.4%)	12 (10.9%)
Prestyloid parapharyngeal space	5 (6.1%)	3 (4.3%)	6 (5.5%)
Prevertebral space	5 (6.1%)	7 (10.1%)	3 (2.7%)
Retropharyngeal space	10 (12.2%)	8 (11.6%)	13 (11.8%)
sublingual space	1 (1.2%)	0 (0.0%)	1 (0.9%)
Total	82 (100%)	69 (100%)	110 (100%)

4.4 Comparison between CT and histopathological findings

Of the 108 participants whose histology examination was successfully done, there was

agreement between CT and histopathology results in 99 (91.7%) of the cases while in

9 (8.3%) of the cases, there was disagreement in the findings **(Figure 12).**
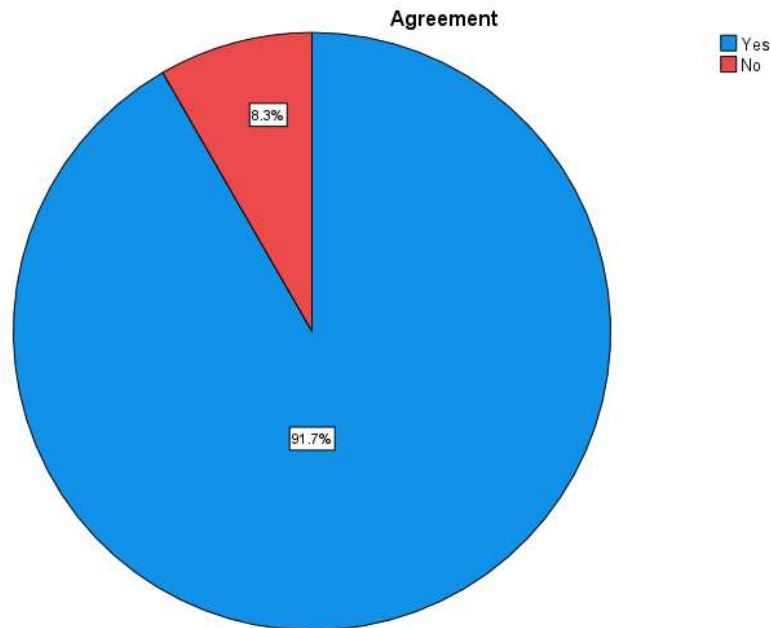
Figure 4.9: Agreement between CT and histopathology results

Of the 9 cases whose diagnosis did not agree, one was diagnosed as parotitis, which

was found to be adenocarcinoma on histopathology. Another was diagnosed as

lymphadenitis, which was confirmed to be accessory parotid tissue on histopathology.

A pleomorphic mixed tumor had been diagnosed as parotitis, hemangioma as

lymphangioma, 2 cases of lymphoma had been diagnosed as oropharyngeal cancer, a

case of lymphoepithelial cyst as an abscess, neurofibroma as a schwannoma and a

case of parotid tumor as a parotid adenopathy (Table 4.6).

Table 4. 6:Discrepancy between CT findings and histological diagnosis

No	CT diagnosis	Histopathology diagnosis
1	Parotitis	Adenocarcinoma
2	Lymphadenitis	accessory parotid tissue
3	Parotitis	pleiomorphic Mixed tumor
4	Lymphangioma	Hemangioma
5	oropharyngeal ca with nodal metastases	non hodgkins lymphoma
6	oropharyngeal ca + nodal metastases	non hodgkins lymphoma
7	parotid adenopathy	Pleomorphic adenoma
8	Schwannoma	Neurofibroma
9	Abscess	lymphoepithelial cysts

The McNemar's test showed that there was no evidence of a statistically significant difference in the proportions of malignant verses benign tumors in the SHN, among patients seen at the radiology department of MTRH in 2016, between imaging and histopathology ($\chi^2_{(1)} = 1.80$, p-value=0.375). Using histopathology as the gold standard showed that imaging had a sensitivity and specificity of 93.2% and 98.2% respectively. In addition, CT imaging had a positive predictive value of 98.2% and a negative predictive value of 93.0%. Table 4.7 below is a contingency table of CT and histopathology.

Table 4. 7: Contingency table of Histopathology and CT scan imaging

		CT Imaging		
		No malignancy	Malignancy	Total
Histology	No malignancy	53 (98.15%)	1 (1.85%)	54 (47.79%)
	Malignancy	4 (6.78%)	55 (93.22%)	59 (52.21%)
	Total	57 (50.44%)	56 (49.56%)	113 (100%)

CHAPTER FIVE: DISCUSSION

5.1 Introduction

Suprahyoid neck masses present a challenge in exploring them using clinical examination; hence, imaging techniques such as CT and MRI are helpful to successfully explore and correctly diagnose these masses(Brown & Harave, 2016; Pynnonen et al., 2017). However, with MRI being expensive and sometimes unavailable in most resource-limited settings, CT remains the best alternative in such settings(Shrestha et al., 2011). In this study, the SHN masses were evaluated using CT. The study consisted of a sample size of 123 patients with SHN masses who were seen at the MTRH radiology unit for a period of one year.

Our study findings showed that the proportion of SHN among men was nearly twice that of women (65% versus 35%). Similar showing results SHN in twice more men than women were observed in 2 separate studies in India (Das & Ghosh, 2020; Kaur et al., 2017). In addition, our findings showed that SHN masses were predominantly observed among adults aged 18-69 years compared to other studies conducted in India showed that most of the patients were aged between 41 and 60 (Kaur et al., 2017; Shrestha et al., 2011). This is could be probable indicator of the potential predominance of SHN in the adult population.

5.2 Radiological characteristics of SHN masses

Key features of the SHN masses identified on CT imaging were enhancement, necrosis, and definition of margins. Well defined margins are indicative of benign lesions while contrast enhancement and necrosis are suggestive of tissue activity and malignancy or inflammatory changes respectively (Kaur et al., 2017). In this study, the proportion of necrosis and well defined margins were 66.7% and 56.7% respectively compared to and 60% and 53% respectively in India for the same

features and a paltry 0.3% for calcification (Kaur et al., 2017). However, in this study no participant with calcification was observed. In addition, Maroldi et al. (2008) found necrosis in 62% and well defined margins in 55% of study participants from North America.

The type of enhancement is essential in the characterization of SHN masses (Aiken & Shatzkes, 2020; Cunqueiro et al., 2019). In this study, about 89% of the participants exhibited enhancement which was classified as heterogeneous, homogeneous or rim. In this study, heterogeneous enhancements were considered indicative of malignancy and was observed in about 49% of the study participants similar to about 47% to 50% that was reported in India (Bakir et al., 2012). On the contrary, a higher proportion of 85% was observed a separate study in India which excluded congenital and traumatic etiologies (Kaur et al., 2017).

5.3 Anatomical locations and patterns of SHN masses

In this study a variety of SHN masses were observed which could be attributed to the different aetiologies. Our study findings showed that more than half (52%) of the SHN masses observed at MTRH in 2016 were found in the pharyngeal mucosal and the parotid spaces. Similarly, about 48% of SHN masses reported by a study in India were observed via CT in the pharyngeal mucosal and the parotid spaces (Kaur et al., 2017). A separate study conducted in Yugoslavia, though with a smaller sample size of 30 patients and using MRI, showed that 30% of SHN masses were located in the same spaces (Semnic et al., 2000). This difference could be attributed to the different population structures between the countries and methodological approaches i.e. Semnic et al., (2000) used MRI compared to CT in this study.

A review of 173 patients, looking at neck masses in general, identified malignant lesions in about 50% of the cases while about a similar proportion of 47% was reported in India (Bakir et al., 2012; Kaur et al., 2017). Coupled with findings from our study showing about 45% malignant SHN masses, these findings outline the important contribution made by malignant tumors to neck masses in general and specifically SHN masses. On the contrary, the same studies identified inflammatory masses as the second most prevalent after malignancy compared to our findings showing benign masses following malignancy in prevalence. In addition, while we observed traumatic mass cases, such were not observed by investigators in India (Kaur et al., 2017). Due to availability of limited literature, comparison of the anatomical locations and patterns of SHN masses and their respective etiologies could not be exhaustively done across different geographies and settings.

Nasopharyngeal cancer was the most common cancer in the pharyngeal mucosal space out of all malignancies identified in this study. On the contrary, oropharyngeal carcinoma was identified as the most prevalent in a separate review (Aiken & Shatzkes, 2020).

At MTRH, metastases from the other regions were the most prevalent diagnosis in the prestyloid parapharyngeal space (PPS). In the USA, benign mixed tumors, especially those of salivary origin, were the most prevalent in the PPS (Stambuk & Patel, 2008). The PPS mainly contains fat with minor salivary glands, is impacted by pathologies originating from neighboring spaces and rarely has a primary pathology primary(Aiken & Shatzkes, 2020). PPS displacement patterns may be indicative of the actual place of origin. If the PPS is anteromedially displaced, that pathology is likely to originate from the parotid space, posteromedially displacement is indicative of masticator space origin, anteriorly displacement is suggestive of carotid space

origin and laterally displacement indicates pathologies of PMS origin (Aiken & Shatzkes, 2020; Koenig et al., 2017).

Despite being the main pathologies in the masticator space, sarcomas accounted for less than 5% and about 11% of all SHN and malignant masses observed in this study. Similarly, primary neoplasm associated with mastication muscles have been found to be rare (Aiken & Shatzkes, 2020). Within the pharyngeal mucosal space, oropharyngeal cancer was the most prevalent malignancy resonating with findings from the study in India (Kaur et al., 2017).

5.4 Agreement between CT and histopathological suprahyoid neck masses diagnosis

A high proportion agreement (92%) was observed between CT and histopathology investigation of 108 participants. Such high proportions of agreement from similar comparative studies, though on about a quarter the number of participants in this study, have been reported in India and Italy at 93% and 96% respectively (Galli et al., 2010; Kaur et al., 2017). In the Indian study, a brachial cleft cyst being misdiagnosed on CT as an abscess and mucoepidermoid carcinoma was misdiagnosed on CT to be pleomorphic adenoma (Kaur et al., 2017). The study in Italy established that a case of salivary gland tumor was wrongly interpreted on CT as a lesion of the Masticator space originating from the mandible (Galli et al., 2010).

CT imaging was shown to be a reliable diagnostic tool for SHN masses at MTRH with high sensitivity (93.2%), specificity (98.2%) positive and negative predictive values of 98.2% and 93% respectively. Similar findings have been reported in three separate studies in India whereby two reported a sensitivity of 96.5% and of specificity 100%, while the other reported sensitivity of 92% and specificity of 87%.

A separate study in Kenya established sensitivity and specificity values of 96.4% and 100% respectively (Muriithi, 2005). The negative and positive predictive values from this study were also consistent with those from the two studies from India which ranged from 97.2% to 100% (Das & Ghosh, 2020; Kaur et al., 2017; Shrestha et al., 2011). In addition, this study has utilized data from a low income setting within the sub-Saharan region to provide further support on the existing evidence on reliability of CT imaging for SHN masses diagnoses (Forghani, 2015; Sekine et al., 2017).

5.5 Limitations of the study

- The many diverse SHN masses make it challenging to carry out an inferential study of the SHN masses.

- Inadequate clinical history from image requests hampers the CT diagnosis process.

CHAPTER SIX: CONCLUSION AND RECOMMENDATIONS

6.1 Conclusion

This study investigated the patterns and anatomical locations of SHN masses among patients seen at MTRH. Therefore, the following conclusions are made:

1. The 3 key features of necrosis, well defined margins and enhancement played an important role in SHN masses differentiation and CT diagnosis. While CT imaging plays a vital role in diagnosis of SHN masses, it is important to carry out histopathological investigations where possible in order to obtain a confirmatory diagnosis.

2. Majority of the SHN masses evaluated were located in the pharyngeal mucosal and the parotid spaces.

3. CT imaging can be used, with high levels of sensitivity and specificity, as a diagnostic tool for SHN masses using histopathology as the gold standard. This is a critical finding that can be used to inform patient management and care for SHN masses, especially in resource constrained settings, considering that histopathology and MRI are more expensive and sparsely available compared to CT. Therefore, hospitals with neither MRI nor histopathology facilities can use the existing CT scan machines to reliably diagnose masses before confirmatory histology is performed. If CT imaging is adopted for SHN mass assessment, patients could gain access to care without hindrance of delayed diagnosis or none at all within the shortest time possible which may lead to better prognosis especially for malignant cases which formed the bulk of SHN masses in this study.

6.2 Recommendations

Based on the evidence from this study, the following recommendations are made:

1. Clinicians could consider using CT imaging for diagnosis of SHN masses to make informed patient management plans before confirmatory histopathology results become available. However, radiologists need to pay attention to the key features identified that can aid in the accurate diagnosis of SHN masses.

2. The government of Kenya, through the ministry of health, could consider drafting a national guideline on usage of CT imaging for the diagnosis of SHN masses. Such efforts could significantly improve on patient care, especially in hospitals without histopathology labs, by utilizing the existing CT imaging infrastructure hence reduced cases of delayed diagnosis or none hence translating to improved patient care and prognosis.

REFERENCES

Adeyi, A., & Olugbenga, S. (2011). The challenges of managing malignant head and neck tumors in a tropical tertiary health center in Nigeria. *The Pan African Medical Journal*, *10*.

Ahuja, A. T., King, A. D., Kew, J., King, W., & Metreweli, C. (1998). Head and neck lipomas: sonographic appearance. *American journal of neuroradiology*, *19*(3), 505-508.

Ali, S. M. H., Kathia, U. M., Gondal, M. U. M., Zil-E-Ali, A., Khan, H., & Riaz, S. (2018). Impact of Clinical Information on the Turnaround Time in Surgical Histopathology: A Retrospective Study. *Cureus*, *10*(5).

Aschenbach, R., Basche, S., Vogl, T. J., & Klisch, J. (2009). Diffusion-Weighted Imaging and ADC Mapping of Head-and-Neck Paragangliomas. *Clinical Neuroradiology*, *19*(3), 215-219.

Ayugi, J., Ogengo, J., Macharia, I., & Olabu, B. (2011). Pattern of acquired neck masses in a Kenyan paediatric population. *International Journal of Oral and Maxillofacial Surgery*, *40*(4), 384–387.

Babbel RW, Harnsberger HR. The parapharyngeal space: the key to unlocking the suprahyoid neck. Semin Ultrasound CTMR. 1990; 11(6):444-59.39.

Bakir, S., Tanriverdi, M. H., Gün, R., Yorgancilar, A. E., Yildirim, M., Tekbaş, G., Palanci, Y., Meriç, K., & Topçu, İ. (2012). Deep neck space infections: A retrospective review of 173 cases. *American Journal of Otolaryngology*, *33*(1), 56–63.

Balogh, E. P., Miller, B. T., Ball, J. R., Care, C. on D. E. in H., Services, B. on H. C., Medicine, I. of, & The National Academies of Sciences, E. (2015). The Diagnostic Process. In *Improving Diagnosis in Health Care*. National Academies Press (US).

Bannister LH, Berry MM, Collins P, et al. Gray's Anatomy, 38thedition. Edinburg, Scotland: Churchill Livingston; 1999.2. Carlson GW. Surgical anatomy of the neck. Surg Clin NorthAm. 1993; 73(4):837-52.3. Gardner M. Basic Anatomy of the Head and Neck. Philadelphia, PA, USA: Lea and Febiger; 1992.4.

Baum, U., Greess, H., Lell, M., Nömayr, A., & Lenz, M. (2000). Imaging of head and neck tumors--methods: CT, spiral-CT, multislice-spiral-CT. *European Journal of Radiology*, *33*(3), 153–160.

Becker MB, Zhären P, Hermans R, et al. Necrotizing fasciitis of the head and neck: role of CT in diagnosis and management. *Radiology.* 1997; 202(2):471-6.36.

Benediktsson, H., Whitelaw, J., & Roy, I. (2007). Pathology Services in Developing Countries: A Challenge. *Archives of Pathology & Laboratory Medicine*, *131*(11), 1636–1639.

Benjamin Odhiambo Bonyodon. (2015). *Imaging patterns of thoracic injuries among patients aged 14 years and above at MTRH, Eldoret, Kenya.* [Thesis, Moi University].

Bisdas, S., Baghi, M., Huebner, F., Mueller, C., Knecht, R., Vorbuchner, M., ... & Vogl, T. J. (2007). In vivo proton MR spectroscopy of primary tumours, nodal and recurrent disease of the extracranial head and neck. *European radiology*, *17*(1), 251-257.

Borner, U., Stow, N. W., & Landis, B. N. (2016). Pleomorphic Adenoma of the Parotid Gland. *The American Journal of Medicine*, *129*(1), e1–e2.

Brand, N. R., Wolf, N., Flanigan, J., Njoroge, R., & Karagu, A. (2017). Histology and Cytopathology Capacity in the Public Health Sector in Kenya. *Journal of Global Oncology*, *4*, 1–7.

Brodsky JR, Kim DY, Jiang Z, et al. Cervical lipoblastoma: case report, review of literature, and genetic analysis. Head Neck.2007; 29(11):1055-60.

Brown, R. E., & Harave, S. (2016). Diagnostic imaging of benign and malignant neck masses in children—a pictorial review. *Quantitative Imaging in Medicine and Surgery*, *6*(5), 591–604.

Cazzato, R. L., Garnon, J., Shaygi, B., Koch, G., Tsoumakidou, G., Caudrelier, J., Addeo, P., Bachellier, P., Namer, I. J., & Gangi, A. (2018). PET/CT-guided interventions: Indications, advantages, disadvantages and the state of the art. *Minimally Invasive Therapy & Allied Technologies*, *27*(1), 27–32.

Chengazi, H. U., & Bhatt, A. A. (2019). Pathology of the carotid space. *Insights into Imaging*, *10*. https://doi.org/10.1186/s13244-019-0704-z

Chong VF, Fan YF, Khoo JB. Nasopharyngeal carcinoma with intracranial spread: CT and MR characteristics. J ComputAssist Tomogr. 1996; 20(4):563-9.43.

Chong VF, Fan YF, Khoo JB. Retropharyngeal lymphadenopathy in nasopharyngeal carcinoma. Euro J Radiol. 1995; 21(2):100-5.20.

Chong VF, Fan YF. Pictorial review: radiology of the masticator space. Clin Radiol. 1996; 51(7):457-65.31.

Chong VF, Fan YF. The retropharyngeal space: route of tumor spread. Clin Radiol. 1998; 53(1):64-7.35.

Chong, V. F. H., Mukherji, S. K., & Goh, C. H. K. (1999). The suprahyoid neck: normal and pathological anatomy. *The Journal of Laryngology & Otology*, *113*(6), 501-508.

Chung, C. J., Armfield, K. B., Mukherji, S. K., Fordham, L. A., & Krause, W. L. (1999). Cervical neurofibromas in children with NF-1. *Pediatric radiology*, *29*(5), 353-356.

Coit, W. E., Harnsberger, H. R., Osborn, A. G., Smoker, W. R., Stevens, M. H., & Lufkin, R. B. (1987). Ranulas and their mimics: CT evaluation. *Radiology*, *163*(1), 211-216.

Colreavy, M. P., Lacy, P. D., Hughes, J., Bouchier-Hayes, D., Brennan, P., O'dwyer, A. J., ... & Walsh, M. A. (2000). Head and neck schwannomas–a 10 year review. *The Journal of Laryngology & Otology*, *114*(2), 119-124.

Cunqueiro, A., Gomes, W. A., Lee, P., Dym, R. J., & Scheinfeld, M. H. (2019). CT of the Neck: Image Analysis and Reporting in the Emergency Setting. *RadioGraphics*, *39*(6), 1760–1781.

Curvo-Semedo, L., Diniz, M., Migueis, J., Julião, M. J., Martins, P., Pinto, A., & Caseiro-Alves, F. (2006). USPIO-enhanced magnetic resonance imaging for nodal staging in patients with head and neck cancer. *Journal of Magnetic Resonance Imaging: An Official Journal of the International Society for Magnetic Resonance in Medicine*, *24*(1), 123-131.

Das, R., & Ghosh, A. (2020). *Role of Multi-slice Spiral Ct in Evaluation of Neck Mass with Cytological Correlation*.

Davis WL, Smoker WR, Harnsberger HR. The normal and diseased infrahyoid retropharyngeal, danger, and prevertebral spaces. Semin Ultrasound CT MR. 1991; 12(3):241-56.9.

De Bondt, R. B. J., Hoeberigs, M. C., Nelemans, P. J., Deserno, W. M. L. L. G., Peutz-Kootstra, C., Kremer, B., & Beets-Tan, R. G. H. (2009). Diagnostic accuracy and additional value of diffusion-weighted imaging for discrimination of malignant cervical lymph nodes in head and neck squamous cell carcinoma. *Neuroradiology*, *51*(3), 183-192.

Dive, A. M., Bodhade, A. S., Mishra, M. S., & Upadhyaya, N. (2014). Histological patterns of head and neck tumors: An insight to tumor histology. *Journal of Oral and Maxillofacial Pathology: JOMFP*, *18*(1), 58–68.

Emonts P, Bourgeois P, Lemort M, et al. Functional imaging of head and neck cancers. Curr Opin Oncol. 2009; 21(3):212-7.18.

Fernandes, T., Lobo, J. C., Castro, R., Oliveira, M. I., & Som, P. M. (2013). Anatomy and pathology of the masticator space. *Insights into Imaging*, *4*(5), 605–616.

Forghani, R. (2015). Advanced dual-energy CT for head and neck cancer imaging. *Expert Review of Anticancer Therapy*, *15*(12), 1489–1501.

Freling, N. J., Molenaar, W. M., Vermey, A., Mooyaart, E. L., Panders, A. K., Annyas, A. A., & Thijn, C. J. (1992). Malignant parotid tumors: Clinical use of MR imaging and histologic correlation. *Radiology*, *185*(3), 691–696.

Fruin ME, Smoker WR, Harnsberger HR. The carotid space in the suprahyoid neck. Semin Ultrasound, CT MR.1990; 11(6):504-19.34.

Galli, F., Flor, N., Villa, C., Franceschelli, G., Pompili, G., Felisati, G., Biglioli, F., & Cornalba, G. (2010). The masticator space. Value of computed tomography and magnetic resonance imaging in localisation and characterisation of lesions. *Acta Otorhinolaryngologica Italica*, *30*(2), 94–99.

Gamss, C., Gupta, A., Chazen, J. L., & Phillips, C. D. (2015). Imaging Evaluation of the Suprahyoid Neck. *Radiologic Clinics*, *53*(1), 133–144.

Gervasio, A., D'Orta, G., Mujahed, I., & Biasio, A. (2011). Sonographic anatomy of the neck: The suprahyoid region. *Journal of Ultrasound*, *14*(3), 130–135.

Ginat, D. T., & Gupta, R. (2014). Advances in Computed Tomography Imaging Technology. *Annual Review of Biomedical Engineering*, *16*(1), 431–453.

Godwin J. Benign lymphoepithelial lesion of the parotid gland adenolymphoma, chronic inflammation, lymphoepithelioma, lymphocytic tumor, Mikulicz disease. Cancer. 1952; 5(6):1089-103.29.

Guerrisi, A., Marin, D., Nelson, R. C., De Filippis, G., Di Martino, M., Barnhart, H., Masciangelo, R., Guerrisi, I., Passariello, R., & Catalano, C. (2011). Effect of varying contrast material iodine concentration and injection technique on the conspicuity of hepatocellular carcinoma during 64-section MDCT of patients with cirrhosis. *The British Journal of Radiology*, *84*(1004), 698–708.

Gupta P, Bhargava SK, Mehrotra G, & Rathi V. (2013). *Role of multi-slice spiral CT in the evaluation of neck masses.26* (1), 51–54.

Haque, M. Z., Karim, M. E., Al-Azad, S., & Mahmood-uz-jahan, null. (2010). Role of computed tomography in the evaluation of pediatric brain tumor. *Bangladesh Medical Research Council Bulletin*, *36*(3), 89–92.

Hardin CW, Harnsberger HR, Osborn AG, et al. Infections and tumors of the masticator space: CT evaluation. Radiology.1985; 157(2): 413-7.32.

Harnsberger HR. The normal and diseased carotid space. In: Handbook of Head and Neck Imaging, 2nd edition. Chicago, IL, USA: Mosby Year Book; 1995.33.

Hodler, J., Kubik-Huch, R. A., & Schulthess, G. K. von (Eds.). (2020). *Diseases of the Brain, Head and Neck, Spine 2020–2023: Diagnostic Imaging*. Springer International Publishing.

Imhof, H., Czerny, C., & Dirisamer, A. (2003). Head and neck imaging with MDCT. *European Journal of Radiology*, *45 Suppl 1*, S23-31.

Jacob, S. (2008). Chapter 7—Head and neck. In S. Jacob (Ed.), *Human Anatomy* (pp. 181–225). Churchill Livingstone.

Jo, B. G., Song, Y. G., Shim, S. G., & Kim, Y. W. (2016). Comparison of enhancement and image quality: Different iodine concentrations for liver on 128-slice multidetector computed tomography in the same chronic liver disease patients. *The Korean Journal of Internal Medicine*, *31*(3), 461–469.

John R. Haaga & Daniel T. Boll. (2017). *CT and MRI of the Whole Body* (6th ed.). Elsevier.

Kadom, N., & Lee, E. Y. (2012). Neck masses in children: Current imaging guidelines and imaging findings. *Seminars in Roentgenology*, *47*(1), 7–20.

Kamel, H. M. (2011). Trends and Challenges in Pathology Practice. *Sultan Qaboos University Medical Journal*, *11*(1), 38–44.

Kaur, R., Singh, P., Kaur, N., Bhatnagar, S., & Dahuja, A. (2017). Role of Computed Tomography (CT) in Localisation and Characterisation of Suprahyoid Neck Masses. *Polish Journal of Radiology*, *82*, 263–270.

Kimura, Y., Sumi, M., Sakihama, N., Tanaka, F., Takahashi, H., & Nakamura, T. (2008). MR imaging criteria for the prediction of extranodal spread of metastatic cancer in the neck. *American journal of neuroradiology*, *29*(7), 1355-1359.

Koeller, K. K., Alamo, L., Adair, C. F., & Smirniotopoulos, J. G. (1999). From the Archives of the AFIP: Congenital cystic masses of the neck: Radiologic‐pathologic correlation. *Radiographics*, *19*(1), 121-146.

Koenig, L. J., Tamimi, D., Petrikowski, C. G., Perschbacher, S. E., Ruprecht, A., Benson, B. W., Hatcher, D., Potter, B. J., & Harnsberger, H. R. (Eds.). (2017). Parapharyngeal Space. In *Diagnostic Imaging: Oral and Maxillofacial (Second Edition)* (pp. 168–171). Elsevier.

Korir, G. K., Wambani, J. S., & Korir, I. K. (2012). Patient doses using multidetector computed tomography scanners in Kenya. *Radiation Protection Dosimetry*, *151*(2), 267–271.

Kresnik, E., Mikosch, P., Gallowitsch, H. J., Kogler, D., Wiesser, S., Heinisch, M., Unterweger, O., Raunik, W., Kumnig, G., Gomez, I., Grünbacher, G., & Lind, P. (2001). Evaluation of head and neck cancer with 18F-FDG PET: A comparison with conventional methods. *European Journal of Nuclear Medicine*, *28*(7), 816–821.

Kropotov, J. D. (2016). Chapter 1.4—Positron Emission Tomography. In J. D. Kropotov (Ed.), *Functional Neuromarkers for Psychiatry* (pp. 27–30). Academic Press.

Lee, Y. Y., Van Tassel, P., Nauert, C., North, L. B., & Jing, B. S. (1987). Lymphomas of the head and neck: CT findings at initial presentation. *American Journal of Roentgenology*, *149*(3), 575-581.

Malone, B., & Baker, S. R. (1984). Benign pleomorphic adenomas in children. *Annals of Otology, Rhinology & Laryngology*, *93*(3), 210-214.

Mancuso AA, Hanafee WN. Nasopharynx and parapharyngealspace: computed tomography and magnetic resonance. In: Imaging of the Head and Neck, 2nd edition. Baltimore, USA: Williams and Wilkins; 1985. pp. 428-97.25.

Manohar B. Kachare & Amarnath R. Mohan. (2017). *Role of computed tomography in the evaluation of neck masses*. *05*(07).

Maroldi, R., Farina, D., Borghesi, A., Marconi, A., & Gatti, E. (2008). Perineural tumor spread. *Neuroimaging clinics of North America*, *18*(2), 413-429.

McHugh, K., & Boothroyd, A. E. (1999). The role of radiology in childhood rhabdomyosarcoma. *Clinical radiology*, *54*(1), 2-10.

Meuwly, J. Y., Lepori, D., Theumann, N., Schnyder, P., Etechami, G., Hohlfeld, J., & Gudinchet, F. (2005). Multimodality imaging evaluation of the pediatric neck: techniques and spectrum of findings. *Radiographics*, *25*(4), 931-948.

Michael, A. S., Mafee, M. F., Valvassori, G. E., & Tan, W. S. (1985). Dynamic computed tomography of the head and neck: differential diagnostic value. *Radiology*, *154*(2), 413-419.

Mohamed, A. A., Oduor, C., & Kinyanjui, D. (2020). HIV-associated neurocognitive disorders at Moi teaching and referral hospital, Eldoret, Kenya. *BMC neurology*, *20*(1), 1-11.

Mukherji, S. K., & Castillo, M. (1998). A SIMPLIFIED APPROAC TO THE SPACES OF THE SUPRAHYOID NECK. *Radiologic Clinics of North America*, *36*(5), 761-780.

Muriithi, I. M. (2005). *The role of CT scan in imaging neck structures and lesions: A radiological - histopathological correlation retrospective study at Kenyatta National Hospital* [Thesis, University of Nairobi].

Onyango, J. F., & Macharia, I. M. (2006). Delays in diagnosis, referral and management of head and neck cancer presenting at Kenyatta National Hospital, Nairobi. *East African Medical Journal*, *83*(4), 85–91.

Patel, N. D., van Zante, A., Eisele, D. W., Harnsberger, H. R., & Glastonbury, C. M. (2011). Oncocytoma: The vanishing parotid mass. *AJNR. American Journal of Neuroradiology*, *32*(9), 1703–1706.

Patterson HC, Kelly JH, Strome M. Ludwig's angina: an update. Laryngoscope. 1982; 92(4):370-8.30.

Peter M. Som & Hugh D. Curtin. (2011). *Head and Neck Imaging* (5th ed.). Elsevier.

Pratap, V., Jain, S. K., Choudhary, A. K., & Prakash, O. (2013). Ultrasonography, Computed tomography, Malignancy. *Efficacy evaluation of ultrasonography and computerized tomography in palpable neck masses*, *2220*.

Pynnonen, M. A., Gillespie, M. B., Roman, B., Rosenfeld, R. M., Tunkel, D. E., Bontempo, L., Brook, I., Chick, D. A., Colandrea, M., Finestone, S. A., Fowler, J. C., Griffith, C. C., Henson, Z., Levine, C., Mehta, V., Salama, A., Scharpf, J., Shatzkes, D. R., Stern, W. B., … Corrigan, M. D. (2017). Clinical Practice Guideline: Evaluation of the Neck Mass in Adults. *Otolaryngology–Head and Neck Surgery*, *157*(2_suppl), S1–S30.

Rankin, S. C. (2006). PET in face and neck tumours. *Cancer Imaging*, *6*(Spec No A), S89–S95.

Ravi, N., Lakshmeesha, M. T., Manjappa, B. H., Naveen, K. G., Ramesh, V., & Nagaraj, B. R. (2015). Does MDCT Really Have a Role in the Evaluation of Neck Masses. *SSRG International Journal of Medical Science (SSRG-IJMS)*, *2*(3).

Rea, P. (2016). *Essential clinically applied anatomy of the peripheral nervous system in the head and neck*. Academic Press.

Reiser, M. F., Takahashi, M., Modic, M., & Bruening, R. (2012). *Multislice CT*. Springer Science & Business Media.

Romano, L., Grazioli, L., Bonomo, L., Xu, J.-R., Chen, K.-M., Dore, R., Vanzulli, A., & Catalano, C. (2009). Enhancement and safety of iomeprol-400 and iodixanol-320 in patients undergoing abdominal multidetector CT. *The British Journal of Radiology*, *82*(975), 204–211.

Schuknecht, B., Stergiou, G., & Graetz, K. (2008). Masticator space abscess derived from odontogenic infection: imaging manifestation and pathways of extension depicted by CT and MR in 30 patients. *European radiology*, *18*(9), 1972-1979.

Seeram, E. (2013). *Computed Tomography - E-Book: Physical Principles, Clinical Applications, and Quality Control*. Elsevier Health Sciences.

Seifert, G. (1992). Histopathology of malignant salivary gland tumours. *European Journal of Cancer Part B: Oral Oncology*, *28*(1), 49-56.

Shah, R. R., & Lewin, J. S. (1998). Imaging of the infrahyoid neck. *Neuroimaging Clinics of North America*, *8*(1), 219-234.

Sekine, T., Barbosa, F. D. G., Delso, G., Burger, I. A., Stolzmann, P., Ter Voert, E. E., ... & Huellner, M. W. (2017). Local resectability assessment of head and neck cancer: positron emission tomography/MRI versus positron emission tomography/CT. *Head & neck*, *39*(8), 1550-1558.

Semnic, R., Jović, R., Bogdanović, D., & Zvezdin, A. (2000). The value of magnetic resonance imaging in diagnosis and staging of supra-hyoid neck tumors. *Archive of Oncology*, *8*(2), 51-54.

Shahab, R., Heliwell, T., & Jones, A. S. (2005). How we do it: A series of 114 primary pharyngeal space neoplasms. *Clinical Otolaryngology: Official Journal of ENT-UK ; Official Journal of Netherlands Society for Oto-Rhino-Laryngology & Cervico-Facial Surgery*, *30*(4), 364–367.

Shetty, D., Jayade, B. V., Joshi, S. K., & Gopalkrishnan, K. (2015). Accuracy of palpation, ultrasonography, and computed tomography in the evaluation of metastatic cervical lymph nodes in head and neck cancer. *Indian Journal of Dentistry*, *6*(3), 121–124.

Shrestha, M. K., Ghartimagar, D., & Ghosh, A. (2011). Diagnostic accuracy of computed tomogram in the evaluation of a neck mass. *JNMA; Journal of the Nepal Medical Association*, *51*(184), 164–170.

Sitienei, L., Abuya, J., & Chumba, D. (2018). Imaging patterns of liver diseases diagnosed by ultrasound guided liver biopsies at Moi Teaching and Referral Hospital. *East African Medical Journal*, *95*(4), 1493–1501.

Smoker WR. Normal anatomy of the infrahyoid neck: an overview. Semin Ultrasound CT MR. 1991; 12(3):192-203.10.

Som, P. M., Sacher, M., Stollman, A. L., Biller, H. F., & Lawson, W. (1988). Common tumors of the parapharyngeal space: refined imaging diagnosis. *Radiology*, *169*(1), 81-85.

Som, P. M., Shugar, J. M., Sacher, M., Stollman, A. L., & Biller, H. F. (1988). Benign and malignant parotid pleomorphic adenomas: CT and MR studies. *Journal of computer assisted tomography*, *12*(1), 65-69.

Som PM. Lymph nodes of the neck. Radiology.1987; 165(3):593-600.11. Faggioni L, Neri E, Bartolozzi C. CT perfusion of head and neck tumors: how we do it.

Stambuk, H. E., & Patel, S. G. (2008). Imaging of the parapharyngeal space. *Otolaryngologic Clinics of North America*, *41*(1), 77–101, VI.

Stathakios, J., & Carron, M. A. (2020). Anatomy, Head and Neck, Neck Triangle. In *StatPearls*. StatPearls Publishing.

Tarin, D. (2012). Clinical and Biological Implications of the Tumor Microenvironment. *Cancer Microenvironment*, *5*(2), 95–112.

Turkington JR, Paterson A, Sweeney LE, et al. Neck masses in children. Br J Radiol. 2005; 78(925):75-85.22.

Vaquero, J. J., & Kinahan, P. (2015). Positron Emission Tomography: Current Challenges and Opportunities for Technological Advances in Clinical and Preclinical Imaging Systems. *Annual Review of Biomedical Engineering*, *17*, 385–414.

Vidiri, A., Guerrisi, A., Pellini, R., Manciocco, V., Covello, R., Mattioni, O., Guerrisi, I., Giovanni, S. D., Spriano, G., & Crecco, M. (2010). Multi-detector row computed tomography (MDCT) and magnetic resonance imaging (MRI) in the evaluation of the mandibular invasion by squamous cell carcinomas (SCC) of the oral cavity. Correlation with pathological data. *Journal of Experimental and Clinical Cancer Research*, *29*(1), 73.

Wanamaker JR, Kraus DH, Biscotti CV, et al. Undifferentiated nasopharyngeal carcinoma presenting as a parotid mass. Head Neck. 1994; 16(6):589-93.42.

White, T. D., & Folkens, P. A. (2005). Chapter 9—HYOID & VERTEBRAE. In T. D. White & P. A. Folkens (Eds.), *the Human Bone Manual* (pp. 155–180). Academic Press.

Whyte, A., Boeddinghaus, R., & Matias, M. A. T. J. (2017). Diagnostic Imaging Principles and Applications in Head and Neck Pathology. In C. S. Farah, R. Balasubramaniam, & M. J. McCullough (Eds.), *Contemporary Oral Medicine* (pp. 1–80). Springer International Publishing. 3-319-28100-1_6-1

Win T, Lewin JS. Imaging characteristics of carotid body tumors. Am J Otol. 1995; 16(5):325-8.49. Farr HW. Carotid boy tumors: a 40-year study. CA Cancer JClin. 1980; 30(5):260-5.50.

Wittich, G. R., Scheible, W. F., & Hajek, P. C. (1985). Ultrasonography of the salivary glands. *Radiologic Clinics of North America*, *23*(1), 29-37.

Yousem, D. M., Lexa, F. J., Bilaniuk, L. T., & Zimmerman, R. I. (1990). Rhabdomyosarcomas in the head and neck: MR imaging evaluation. *Radiology*, *177*(3), 683-686.

APPENDICES

Appendix I: Consent form

English Version

Investigator: My name is Dr. Titus Ndugire; I am a qualified doctor, registered in Kenya. I am currently pursuing a master's degree in Radiology and Imaging at Moi University. I request to recruit you into my research study on evaluation of CT scan findings of patients with Suprahyoid Neck Masses.

Purpose: This study will seek to evaluate the CT scan findings in patients with suprahyoid neck masses at (MTRH).

Procedure: A CT scan will be carried out and the results evaluated by the researcher.

Risks

There are no risks associated with your participation in this study.

Benefits and Compensations

You will not be compensated for participating in this study and there are no direct benefits for you as an individual participant, however the findings of this study will help understanding the nature and distribution of Suprahyoid neck masses for the purpose of intervention planning and policy development.

Voluntary Participation and Withdrawal

Your participation is entirely voluntary, and should you change your mind, you have the right to withdraw from participating in the study at any time without penalty.

Confidentiality

All data will be kept under lock and key and will only be accessible to those involved in the data collection. Electronic files will be saved on Password. There will be no way to identify individual participants. We will not identify you or use any information that would make it possible for anyone to identify you in any presentations or written reports about this study.

Rights to Refuse: Participation in this study is voluntary, there is freedom to refuse to take part or withdraw at any time. This study has been approved by the Institutional

Research and Ethics Committee (IREC) of Moi University/Moi Teaching and Referral Hospital.

Confirmation of Consent

Are you willing to participate in this study?

Yes_____ No_____

If yes, please sign (Parent or guardian to sign on behalf of children below 18 years).

Name:

_____Sign:_____Time_____Date_____

Researcher:

_____Sign:_____Time_____Date_____

Kiswahili Version

Mpelelezi: jina langu ni Daktari Titus Ndugire.Mimi ni daktari aliyehitimu na kusajiliwa na bodi ya Kenyaya Madaktari na Madaktari wa meno.Mimi sasa natafuta shahada ya uzamili katika Radiology na Imaging katika Chuo Kikuu cha Moi. Ningependa kukuhusisha katika utafiti wangu ambao ni kuchunguza uvimbe unaopatikana ndani mwa shingo nikitumia mashine ya CT Scan Katika Hospitali Kuu ya MTRH.

Kusudi: Utafiti huu utachunguza matokeo ya CT Scan kwa wagonjwa walio na uvimbe wa ndani mwa shingo katika hospitali kuu ya MTRH.

Utaratibu: utapigwa picha na mashine ya CT na matokeo yataaangaliwa na daktari anayehusika na utafiti huu.

Faida: Kutakuwa hakuna faida moja kwa moja ya kushiriki katika utafiti huu. Wanaofanyiwa utafiti watakuwa nahaki nakupewa ubora sawa na wale ambao hawatofanyiwa utafiti huo.

Hatari: Hakuna hatari ya kutarajia kwa washiriki inatokana na utafiti huu.

Usiri: habari zote zilizopatikana katika utafiti huu wa kutibiwa zitawekwa kwa usiri mkubwa na wala haitatolewa kwa mtu yeyote asiye husika na utafiti.

Haki ya kukataa: Kushiriki katika utafiti huu ni hiari yako, kuna uhuru wa kukataa kuchukua sehemu au kutoka wakati wowote. Utafiti huu umeidhinishwa na Utafiti wa Taasisi na Kamati ya Maadili (IREC) ya Chuo Kikuu cha kufundisha cha Moi na Hospitali kuu ya Rufaa.

Weka sahihi au kufanya alama kama unakubali kushiriki katika utafiti

Mgonjwa / Mlezi: .... Mpelelezi: ....

Tarehe: ....

Appendix II: Data collection tool

1) Patient No. ------------------------

2) Age years   ………………………….

3) Sex ………………………………………

4) Features of mass as assessed by CT (size, site, margins, enhancement characteristics)

………………………………………………………………………………………………
…………………………………..

5) Is the Disease Process Confined to The Space?

a) Yes   b) No

6) Imaging Diagnosis

………………………………………………………………………………………………
………………………………………………………………………………………………
………………………………………………………………………………………………
………………………………………………………………………………………………
………………………………………………………………………………………………
………………………………………………………………………

7) Histopathological Diagnosis

………………………………………………………………………………………………
………………………………………………………………………………………………
………………………………………………………………………………………………
………………………………………………………………………………………………
………………………………………………………………………………………………
…………………………………………………………………………………….

Appendix III: Work plan including time frame

Activity	2018			2018	2018-19	2019	
	Feb	Feb	March	August	Sep – July	August	Sep
Concept Formulation	▓						
Title defence and approval		▓					
Proposal writing and presentation			▓	▓			
Actual data collection					▓		
Data analysis					▓	▓	▓
Report writing and presentation						▓	▓

Appendix IV: Study Schema

```
┌─────────────────────────────────────────────┐
│  Patients presenting with neck masses to the │
│              CT scan unit                     │
│                 n=147                         │
└─────────────────────────────────────────────┘
```

```
┌──────────────────────┐
│ Excluded without SHN │ ◄──────
│ masses n-5           │
└──────────────────────┘
```

```
┌─────────────────────────────────────────────┐
│        Patients with SHN masses n=142         │
└─────────────────────────────────────────────┘
```

```
┌──────────────────────┐
│ Those with prior     │ ◄──────
│ interventions for    │
│ SHN masses n=19      │
└──────────────────────┘
```

```
┌─────────────────────────────────────┐
│ Patient consented, data collected and│
│          analyzed n=123              │
└─────────────────────────────────────┘
```
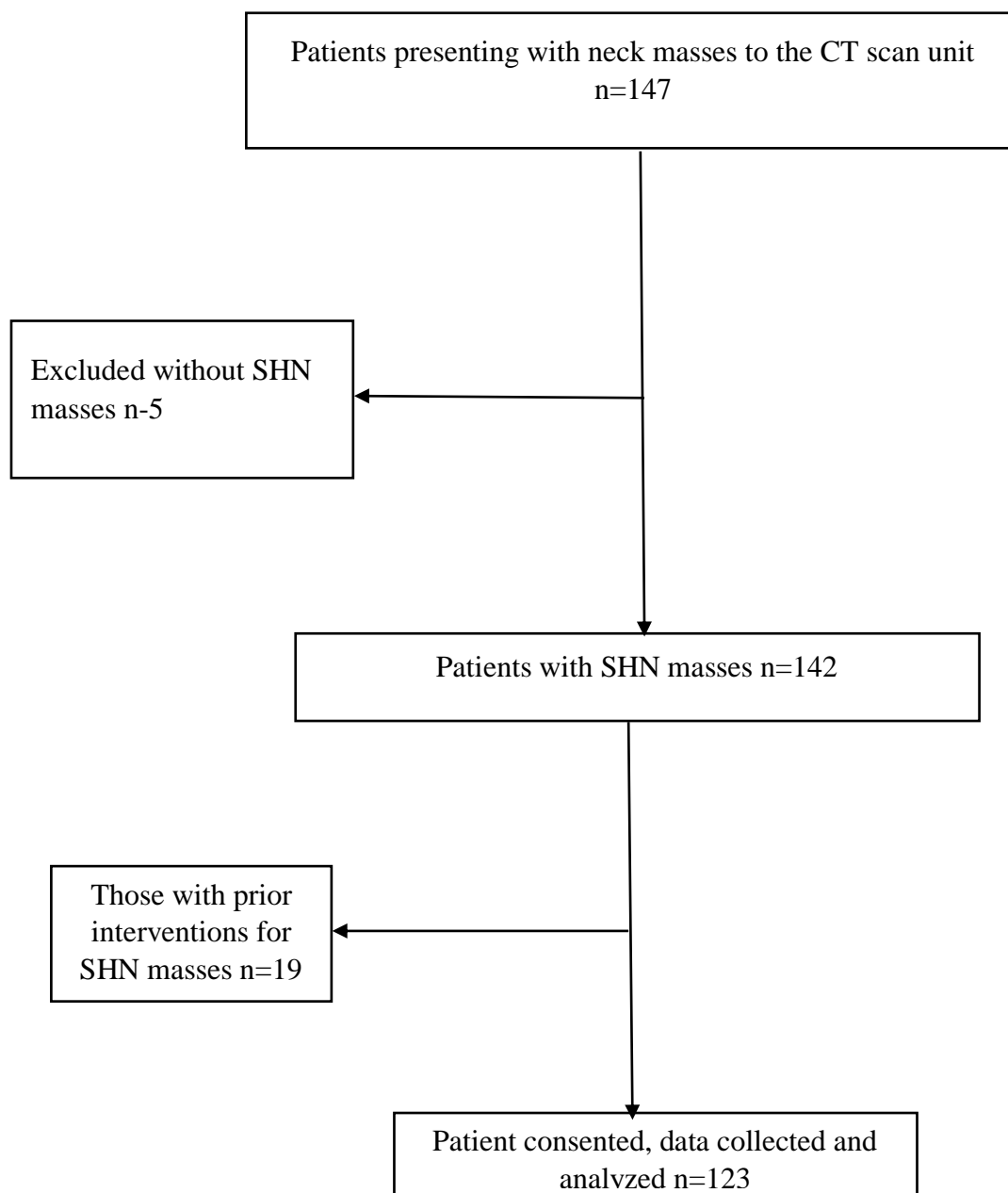
Appendix V: A1: Suprahyoid neck spaces and CT diagnosis

CT diagnosis	Carotid space	Masticator space	Parotid space	Pharyngeal Mucosal space	posterior cervical space	Post styloid parapharyngeal space	Prestyloid parapharyngeal space	Pre-vertebral space	Retropharyngeal space	sublingual space	Total
Abscess	1	3	2	6	1	1	0	0	7	0	21
Brachial cleft cyst	0	0	1	0	0	0	0	0	0	0	1
Ca base of tongue	0	0	0	1	0	0	0	0	0	1	2
Carotid space cellulitis	0	0	0	0	0	2	0	0	0	0	2
Cystic hygroma	0	0	0	0	2	0	0	0	0	0	2
Dermoid cyst	0	0	0	1	0	0	0	0	0	0	1
Fragmented vertebral fracture	0	0	0	0	0	0	0	1	0	0	1
Hematoma	0	0	0	0	1	0	0	0	0	0	1
Internal carotid aneurysm	0	0	0	0	0	1	0	0	0	0	1

Leiomyoma	0	1	0	0	0	0	0	0	0	0	1
Lipoma	0	0	1	0	1	0	1	0	0	0	3
Lymphadenitis	0	1	0	0	0	0	0	0	0	0	1
Lymphadenopathy	0	0	0	1	0	0	0	0	0	0	1
Lymphangioma	0	0	2	0	1	0	0	0	0	0	3
Lymphoma	0	0	0	2	0	0	0	0	0	0	2
Mandibular Osteosarcoma	0	1	0	0	0	0	0	0	0	0	1
Metastases	0	0	0	6	0	0	6	0	5	0	17
Minor salivary gland tumour	0	0	0	1	0	0	0	0	0	0	1
Oropharyngeal cancer	0	0	0	11	0	0	0	0	0	0	11
Osteomyelitis	0	0	0	0	0	0	0	5	0	0	5
Osteosarcoma	0	1	0	0	0	0	0	0	0	0	1
Paraganglioma	0	0	0	0	0	4	0	0	0	0	4
Parotid adenoma	0	0	1	0	0	0	0	0	0	0	1
Parotid adenopathy	0	0	1	0	0	0	0	0	0	0	1
Parotid tumour	0	0	14	1	0	0	0	0	0	0	15
Parotitis	0	0	1	0	0	0	0	0	0	0	1
Reactive adenopathy	0	0	0	0	0	0	0	0	1	0	1

Sarcoma	0	5	0	0	0	0	0	0	0	0	5
Schwannoma	0	0	0	0	0	4	0	0	0	0	4
Sialolithiasis	0	0	1	0	0	0	0	0	0	0	1
Squamous cell ca	0	0	1	3	0	0	0	0	0	0	4
Stensen duct stone	0	0	1	0	0	0	0	0	0	0	1
Tonsillar carcinoma	0	0	0	1	0	0	0	0	0	0	1
Tonsillitis	0	0	0	4	0	0	0	0	0	0	4
Vertebral fracture with soft tissue swelling	0	0	0	0	0	0	0	1	0	0	1
Total	**1**	**12**	**26**	**38**	**6**	**12**	**7**	**7**	**13**	**1**	**123**

Appendix VI: IREC APPROVAL

MU/MTRH-INSTITUTIONAL RESEARCH AND ETHICS COMMITTEE (IREC)

MOI TEACHING AND REFERRAL HOSPITAL
P.O. BOX 3
ELDORET
Tel: 33471/I/2/3
Reference: IREC/2018/127
Approval Number: 0003100

MOI UNIVERSITY
COLLEGE OF HEALTH SCIENCES
P.O. BOX 4606
ELDORET
6th September, 2018

Dr. Titus Ndugire,
Moi University,
School of Medicine,
P.O. Box 4606-30100,
ELDORET-KENYA.

INSTITUTIONAL RESEARCH &
ETHICS COMMITTEE
0 6 SEP 2018
APPROVED
P.O. Box 4606-30100 ELDORET

Dear Dr. Ndugire,

RE: FORMAL APPROVAL

The MU/MTRH- Institutional Research and Ethics Committee has reviewed your research proposal titled: -
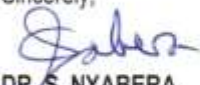
"Patterns of CT Scan Findings in Patients with Suprahyoid Neck Masses at Moi Teaching and Referral Hospital (MTRH)".

Your proposal has been granted a Formal Approval Number: *FAN: IREC 3100* on 6th September, 2018. You are therefore permitted to begin your investigations.

Note that this approval is for 1 year; hence will expire on 5th September, 2019. If it is necessary to continue with this research beyond the expiry date, a request for continuation should be made in writing to IREC Secretariat two months prior to the expiry date. You will be required to submit progress report(s) on application for continuation, at the end of the study and any other times as may be recommended by the Committee.

Furthermore, you must notify the Committee of any proposal change (s) or amendment (s), serious or unexpected outcomes related to the conduct of the study, or study termination for any reason. You will also be required to seek further clearance from any other regulatory body/authority that may be appropriate and applicable to the conduct of this study.

Sincerely,

DR. S. NYABERA
DEPUTY-CHAIRMAN
INSTITUTIONAL RESEARCH AND ETHICS COMMITTEE

cc	CEO	-	MTRH	Dean	-	SOP	Dean	-	SOM
	Principal	-	CHS	Dean	-	SON	Dean	-	SOD

Appendix VII: Hospital Approval

An ISO 9001:2015 Certified Hospital

MOI TEACHING AND REFERRAL HOSPITAL

Telephone :(+254)053-2033471/2/3/4
Mobile: 722-201277/0722-209795/0734-600461/0734-683361
Fax: 053-2061749
Email: ceo@mtrh.go.ke/directorsofficemtrh@gmail.com

Nandi Road
P.O. Box 3 – 30100
ELDORET, KENYA

Ref: ELD/MTRH/R&P/10/2/V.2/2010

14th September, 2018

Dr. Titus Ndugire,
Moi University,
School of Medicine,
P.O. Box 4606-30100,
ELDORET-KENYA.

APPROVAL TO CONDUCT RESEARCH AT MTRH

Upon obtaining approval from the Institutional Research and Ethics Committee (IREC) to conduct your research proposal titled:-

"Patterns of CT Scan Findings in Patients with Suprahyoid Neck Masses at Moi Teaching and Referral Hospital (MTRH)".

You are hereby permitted to commence your investigation at Moi Teaching and Referral Hospital.

CEC
APPROVED
1 4 SEP 2018

DR. WILSON K. ARUASA, *MBS*
CHIEF EXECUTIVE OFFICER
MOI TEACHING AND REFERRAL HOSPITAL

cc - DCEO, (CS)
- Director of Nursing Services (DNS)
- HOD, HRISM

All correspondence should be addressed to the Chief Executive Officer
Visit our Website: www.mtrh.go.ke
TO BE THE LEADING MULTI-SPECIALTY HOSPITAL FOR HEALTHCARE, TRAINING AND RESEARCH IN AFRICA